# "Synthesis and Characterizations of Semiconductor material ($Cu_2ZnSnS_4$) for Solar Cell"

A Thesis Submitted

In partial fulfillment of the requirement

For the degree of

**MASTER OF TECHNOLOGY**

**IN**

**MATERIAL AND METALLURGICAL ENGINEERING**

**BY**

**Shri kant Verma**

**(Roll no. 600902011**

**SCHOOL OF PHYSICS AND MATERIAL SCIENCE**

**THAPAR UNIVERSITY**

**PATIALA-147004, INDIA**

# CERTIFICATE

This is to certify that the thesis entitled **"Synthesis and Characterization of Semiconductor material (Cu2ZnSnS4) for Solar Cell"** submitted by **Mr. Shrikant Verma** is in the partial fulfillment for Degree of MASTER of TECHNOLOGY in MATERIALS and METALLURGICAL ENGINEERING of this university. This work has been done under our supervision. The work presented in this thesis is original to the best of our knowledge and has not been submitted to any other degree of this or any other university.

This work has been carried out from 5 January 2011 to 12 July 2011.


**Dr. Kiran Jain**
Scientist F
Physics of Energy Harvesting Division
National Physical Laboratory
New Delhi-110012

**Dr.D.P.Singh**
Assistant Professor
School of Physics and Material Science
Thapar University
Patiala-147004

**Dr.O.P. Pandey**
Professor and Head
School of Physics and Material Science
Thapar University
Patiala-147004

**Prof. S.K. Mohapatra**
Dean. Academic Affairs
Thapar University
Patiala-147004

# ACKNOWLEDGEMENT

This master thesis work is the final examination toward getting my master degree in Material Science and Engineering at Thapar university (Patiala) Punjab. The work has been carried out within the Centre for organic Electronics at National Physical Laboratory (New Delhi) India. I express my deep sense of gratitude to **Dr. Suresh Chand** for providing me an opportunity to work in Physics Energy Harvesting division, NPL. His astonishing language skills and his clear vision of scientific content help me in tremendous manner. Words can hardly express my sense of gratitude to **Dr. Kiran Jain** for her invaluable supervision during the course of my thesis work. Dr. Jain was always available and helpful. Her great knowledge and wonderful attitude help in my training tremendously; her kindness, patience are much appreciable.

I want to express my deep sense of gratitude to my supervisor **Dr. D.P. Singh**. His wide knowledge and logical way of thinking have been of great value for me.

I express my gratitude to **Dr. O. P Pandey,** Head, School of Physics and Material Science, Thapar University Patiala for his invaluable support and encouragement.

I wish to express my sincere thanks to **Dr. R.C Budhani (Director NPL),** for permitting and providing the facilities necessary for carrying out thesis work at NPL.

**Dr. Rajiv Chopra**, Head HRD group, NPL, for their support and encouragement during the course of thesis work. I am extremely thankful to Dr.Suresh Chand, Dr. S. K. Dhawan, for their invaluable help.

I also want to thanks Mr. Dharamveer Siani, from HRD group for his kind help.

I am deeply indebted to my teachers, Dr. K. K. Raina , Dr. N. K. Verma , Dr. Kulvir Singh , Dr. Sunil Kumar , Dr. Manoj Kumar, Dr. S. D. Tiwari, Dr. Loveleen Kaur , Dr.Alka Upadhaya, Dr. Puneet Sharma, Dr. Bhupendra Kumar Chudasama and Dr.Bansal. Their ideals and concepts have had a remarkable influence on my understanding in the field of Material and Metallurgical Engineering.

I would like to give my special thanks to Tanvi Vats, Mr. Amit Kumar, Abhishek Sharma, Miss. Aneeta Khakar, Miss. Arti Mehta, Arjun yadav, Sumit Kumar, Miss Harjeet, Miss. Parul, Deepak Patel, Richa Sharma, Miss Meenu, Mr. Suresh Kumar,Vijay and Akshay, Arvind, Monti Tyagi, Romi Bharol, Parul Koda, Mukul Verma, Ishvdeep Shokar, Khuswinder Smara, Bipin

Sharma.for their kind support in my work. Miss Poonm and Mr. Alok Kumar Mishra helped me in all possible ways. Their timely discussions are very much appreciable. I also want to thanks my classmates **Mr. Mukul Verma** , Miss Meenu and my junior & training mates .

I want to express my heart full thanks to my most valuable friend **Abhishek Sharma**. In my hard times you pushed me always in the right direction only because of your inspiration. I am going towards successful completion of my M.Tech. Degree.

I wish to express my warm and sincere thanks to all my friends (V. Karthik, Harshit kumar Khandelwal, Lavish kansal, Yogesh Billa, Arti Choudhary, Ragni Sachan).

Who devoted Their Valuable time and help full me in all possible ways towards successful completion of this work.

I owe my most sincere gratitude to my mother, my father, my sister who honest support obstinate love give me energy to complete this work successful and gave me untiring help during my difficult moments. They have always wanted the best for me and I admire my mother determination and sacrifice to me through college.

Lastly I want to thanks Rt. Scientist **Bipin kumar** for their help in arranging apparatus laboratory experiments.

(Shri Kant Verma)

## ABSTRACT

Quaternary kesterite-type $Cu_2ZnSnS_4$ (CZTS) nanoparticles for low-cost thin film solar cell were successfully synthesized using a relatively simple and convenient solvothermal and hydrothermal route without and with nitrogen atmosphere. Nanoparticles with diameters of about 5–10nm were obtained at the temperature of $180^0$C, analyzed by transmission electron microscopy (TEM).The morphologies of the continuous CZTS films with satisfactory stoichiometry were characterized by scanning electron microscopy (SEM) and energy dispersive X-ray analysis (EDXA). The crystallinity of CZTS nanoparticles was greatly improved by annealing in $H_2S$ (5%) /Ar mixed gases analyzed by X-ray diffraction (XRD). High-resolution X-ray photo-emission spectroscopy (XPS) analysis of the four constituent elements confirmed the purity and composition of CZTS nanoparticles. UV–vis absorption spectra measurement indicated that the band gap of as-synthesised CZTS nanoparticles of both was about 1.5eV, which was near the optimum value for photovoltaic solar conversion in a single-band-gap device.

# CONTENTS

## LIST OF FIGURES

.

# INTRODUCTION CHAPTER-1

## 1.1 World Energy Demand and the Necessity of Alternative Energy Sources

The world energy demand is still increasing. At the moment fossil fuels and nuclear energy are the main energy sources. This classical energy sources cannot provide us with enough energy for the future any more. One problem is that the resources are limited. The stock of carbon-based fuels will be exploited in roughly 50 years. Another big problem is that carbon dioxide, the final product of burned fossil fuel, is known to influence earth climate significantly. Nuclear energy has always been subject of intensive public discussion due to the security and health risks of nuclear power stations and the following problems with radioactive waste. To solve these problems, big efforts have been made to develop new, alternative energy sources over the last decades.

One of this alternative energy sources is solar energy. The sun is the ideal energy source. It is reliable, clean, for free and can be used all over the whole world. The direct conversion of sunlight into electricity by photovoltaic cells is widely used in the meantime. More energy from sunlight strikes the Earth in 1 hour than all the energy consumed on the planet in a year. But even though solar energy offers a natural and environmentally-friendly solution to our increasing energy needs, it currently provides only about 1 millionth of the total electricity supply, and that is mainly because of the high cost associated with solar electricity. Most solar cells are made with silicon, and both the cost of the raw material and the cost of manufacturing conspire to keep prices high and limit the possibility of photovoltaic (PV) power from becoming competitive with hydro, fossil and nuclear energy. It is estimated that in order to be competitive, the cost/watt of solar panel needs to be dramatically reduced by approximately a factor of 5–10 to compete with electricity generated by fossil fuels or nuclear power.

In India photovoltaic modules with a power output of 50 MW (peak) have been installed till the end of 2012. The main part of the installed modules is based on silicon. The production costs of silicon solar cells are high due to the very high energy intensive production. Therefore thin film technique should reduce material consumption and

production costs. For these techniques inorganic semiconductors like amorphous or polycrystalline silicon, cadmium telluride or copper indium diselenide and disulphide or organic semiconductors can be used. For organic solar cells or hybrid solar cells very cheap coating techniques like spin coating, doctor blading, ink jet printing, etc. are available. The development of clean energy resources as an alternative to the fossil fuel has become one of the most important tasks assigned to the researchers from modern science and technology in the 21st century. Among a wide variety of renewable energy sources, solar energy is the best alternative, suitable for meeting the energy demands of the modern society.

**Review:**

$CuInSe_2$-based chalcopyrite semiconductors has proved to be successful candidates for terrestrial photo voltaic (PV).Cu (In,Ga) $Se_2$ (CIGSe) thin film solar cells exhibited a record conversion efficiency of 19.9% [1]. These cells utilize expensive and scarce elements like indium, which affects large-scale production. To achieve the goal of cost-effective photo voltaic technology, it is necessary to explore new materials like $Cu_2ZnSnSe_4$, $Cu_2ZnSnS_4$ and other quaternaries of these chalcopyrite-like semiconductors. The elements zinc and tin in these compound semiconductors are relatively cheap and abundant compared to indium and gallium used in CIGS thin film solar cells. In order to promote the use of photovoltaic devices, it is necessary to develop the solar cells with low cost, high efficiency, and less environmental damaging. A quaternary $Cu_2ZnSnS_4$ (CZTS) thin film is a promising candidate for low cost absorber layer in thin film solar cell due to its excellent material properties for obtaining high efficiency such as suitable band gap energy of 1.4–1.5 eV, and large absorption coefficient over $10^4$ $cm^{-1}$[2,3].

In addition, this compound does not contain toxic elements such as Se or Cd and expensive rare metals, resulting in realizing a solar cell with less environmental damaging and low cost. Figure 1.1 Shows the Shockley-Queisser limit for the maximum possible efficiency of a solar cell. X-axis is the band gap of the solar cell; the y-axis is the highest possible efficiency (ratio of electrical power output to light power input (Assumes a single-junction solar cell under un-concentrated light and some other assumptions too.)

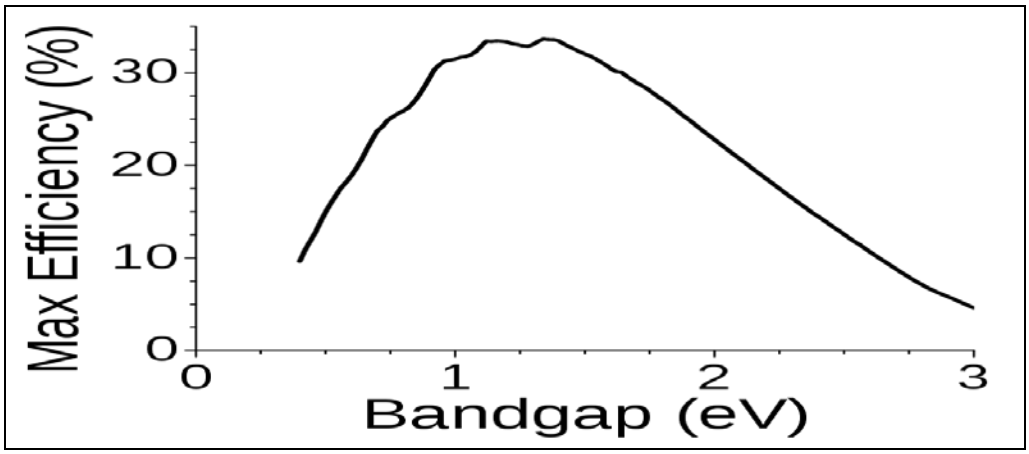


**Figure 1.1 The Shockley-Queisser limits for the maximum possible efficiency of a Solar cell.**

A various physical and chemical techniques like, atom beam sputtering [4], hybrid sputtering [5], RF magnetron sputtering [6], thermal evaporation [7], pulsed laser deposition [8,9], sulfurization of electron-beam-evaporated precursors [10,11], spray pyrolysis [12,13], sol–gel sulfurizing method [14], etc. have been used for the synthesis of CZTS thin films for solar cell applications.

However, these methods have some drawbacks such as expensive precursors, complicated apparatus and even some toxic byproducts evolved during their synthesis. In addition, these methods are performed at high temperatures, which results in inter-diffusion of the component elements, and degrading the device quality structures [15].

Solar cells based on $Cu_2ZnSnSe_4$ (CZTSe) have achieved power conversion efficiencies as high as 9.6% under AM1.5G illumination and In figure1.1Shockley–Queisser photon balance calculations indicate that the theoretical limit for $Cu_2ZnSnS_4$ (CZTS) thin film solar cell is32.2% [16,17].

The present work is related with the synthesis of good quality CZTS nanoparticles by a simple solvothermal and hydrothermal method with and without nitrogen atmosphere. The physical properties of the CZTS nanoparticals, such as stoichiometric

composition, structure, morphology and absorption characteristics were well studied. As-synthesised CZTS nanoparticles that was coated on a substrate and sintered into bulk material to prepare large-area uniform precursor films with low-cost source materials and capital equipment.

## 1.2. History of kesterite-related PV materials:

### 1.2.1 Kesterite-related compounds and structures

Chalcogenide compounds with a $Cu_2(M_{II})(M_{IV})(S,Se)_4$ ($M_{II}$=Mn, Fe, Co, Ni, Zn, Cd, Hg; $M_{IV}$=Si, Ge, Sn) stoichiometry have been of interest for many years because of their appearance as naturally occurring minerals and also suitable for direct band gaps for application in solar cells and other optical devices [18–23]. The zinc blende (or sphalerite)-related structures adopted by these compounds depend on the degree and type of metal cation ordering within the face-centered cubic (fcc) array of chalcogenide anions (with both metals and chalcogens adopting a tetrahedral coordination). One way of viewing these structures is by starting from the ternary chalcopyrite structure (Fig. 1.2), $CuM_{III}(S,Se)_2$, and replacing the trivalent $M_{III}$ ions with an equal number of divalent $M_{II}$ and tetravalent $M_{IV}$ metals. When the ordering of the metals is such that Cu and $M_{IV}$ atoms alternate on the z=0 and ½ (z=fractional coordinate along the long c-axis of the structure) planes and Cu and $M_{II}$ atoms alternate on the z=¼ and 3/4 planes, this is known as the kesterite structure, whereas when $M_{II}$ and $M_{IV}$ atoms alternate on the z=0 and ½ planes and only Cu resides on the z=¼ and ¾ planes, this is known as the stannite structure. While the kesterite structure has the same basic Cu/S structure as chalcopyrite, the stannite structure requires some reorganization of the Cu sub-lattice. Figure.1.2 shows schematic representation of the chalcopyrite structure (drawn with $M_{III}$=In), and kesterite and stannite structures (drawn with $M_{II}$=Zn, $M_{IV}$=Sn). The unit cell boundaries are denoted with dashed lines and the space group for each structural type is also provided.

Note that determining whether a structure adopts a kesterite or stannite structure is difficult to do without careful single crystal structural analysis or Rietveld-type analysis using X-ray and/or neutron diffraction data, which has not been completed for most of

the compound, is in the above series. Two counter-examples are $Cu_2FeSn(S,Se)_4$, which has been determined to be stannite [19], and $Cu_2ZnSnS_4$ (CZTS), which was originally described as stannite, but is now recognized as kesterite [19,24,25]. $Cu_2ZnSnSe_4$ (CZTSe) has also been described as stannite in the literature [20, 26–28]. However, the data presented for this compound were largely powder X-ray diffraction (XRD) data, which cannot reliably be used to distinguish between the two possibilities. Theoretical calculations predict that the lowest energy configuration for CZTSe (as for CZTS) is kesterite [26,29], although the difference in energy between kesterite and stannite is much smaller for the selenide vs. the sulfide, suggesting a stronger tendency of the selenide to incorporate stacking faults involving alternative layering sequences. We will describe all compounds in the $Cu_2ZnSn(S,Se)_4$ (CZTSSe) family as kesterite, with the recognition that experimental verification of this assignment for the high Se-content samples must still be provided. Lattice constants and band gaps of several more thoroughly studied kesterites and stannites are given in Table 1.

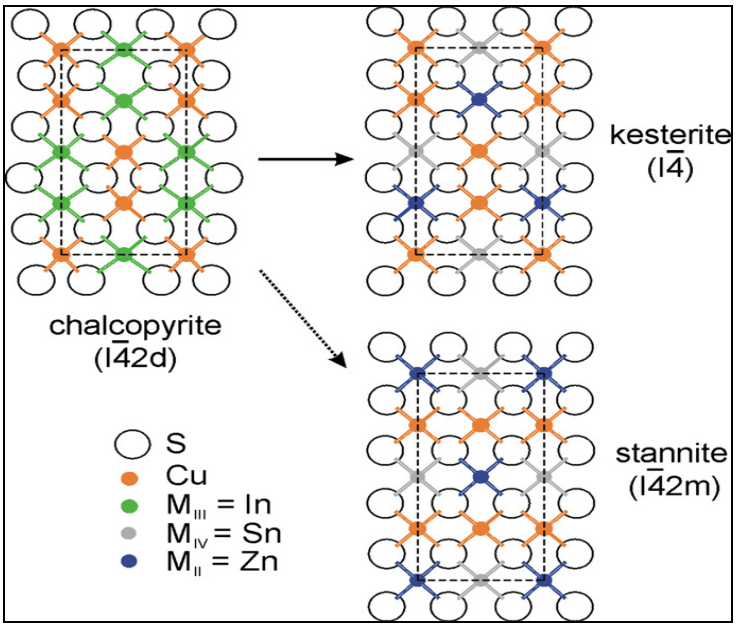


**Figure.1.2 Schematic representation of the chalcopyrite structure , and kesterite and stannite structures.**

**Table 1** Lattice constants and band gaps for selected families of kesterite/stannite materials for which both structural and band gap information have been reported.

| Compound | a (˚A) | c (˚ A) | V (˚$A^3$) | Eg (eV) | References |
|---|---|---|---|---|---|
| $Cu_2ZnSnS_4$ | 5.427 | 10.848 | 319.5 | | [23] |
| | 5.432 | 10.840 | 319.9 | | [30] |
| | 5.435 | 10.822 | 319.7 | | [31] |
| | 5.426 | 10.81 | 318.3 | 1.45 | [32] |
| | | | | 1.45 | [33] |
| | | | | 1.51 | [34] |
| $Cu_2ZnSn(Se_{2.4}S_{1.6})$ | 5.567 | 11.168 | 346.1 | 1.21 | [30] |
| $Cu_2ZnSn(Se_{3.9}S_{0.1})$ | 5.668 | 11.349 | 364.6 | 1.03 | [30] |
| $Cu_2ZnSnSe_4$ | 5.681 | 11.34 | 366.0 | | [18] |
| | 5.684 | 11.353 | 366.8 | 0.94 | [35] |
| | 5.688 | 11.338 | 366.8 | | [27] |
| | | | | 1.017 | [36] |
| $Cu_2ZnGeS_4$ | 5.341[a] | 10.509[a] | 299.8 | | [37] |
| | 5.344 | 10.513 | 300.2 | | [31] |
| $Cu_2ZnGeSe_4$ | 5.622 | 11.06 | 349.6 | | [18] |
| | 5.606 | 11.042 | 347.0 | 1.63 | [20] |
| | 5.618 | 11.04 | 348.4 | 1.52 | [38] |
| $Cu_2CdSnS_4$ | 5.586 | 10.834 | 338.1 | | [23] |
| | 5.593 | 10.840 | 339.1 | | [31] |
| | | | | 1.06 | [33] |
| | | | | 1.16 | [39] |
| $Cu_2CdSnSe_4$ | 5.832 | 11.389 | 387.4 | 0.96 | [20] |
| | | | | 0.89 | [40] |
| | 5.829 | 11.418 | 388.0 | | [27] |
| | 5.832 | 11.392 | 387.5 | | [31] |
| | 5.814 | 11.47 | 387.7 | | [18] |
| $Cu_2CdGeSe_4$ | 5.657 | 10.988 | 351.6 | | [23] |
| | | | | 1.29 | [40] |

[a]Also reported [23] as orthorhombic with lattice constants a=7.504 A˚ b=6.474 A˚, c=6.185 A˚.

### 1.2.2. Kesterite-related photovoltaic films

Table 1 demonstrates that many of the kesterite-related phases exhibit a direct band gap in the optimal range for photovoltaic energy conversion (all are reported to be p-type semiconductors). Despite this fact, relatively few of these compounds have been reported in actual solar cell devices. In 1988, Ito et al. [33] examined the electrical and optical properties of CZTS, a material which has all earth-abundant and relatively non-toxic elements, as well as $Cu_2CdSnS_4$ (CCTS). Both compounds were reported to be direct band gap p-type semiconductors with band gaps of 1.45 and 1.06 eV for the zinc and cadmium compounds, respectively.

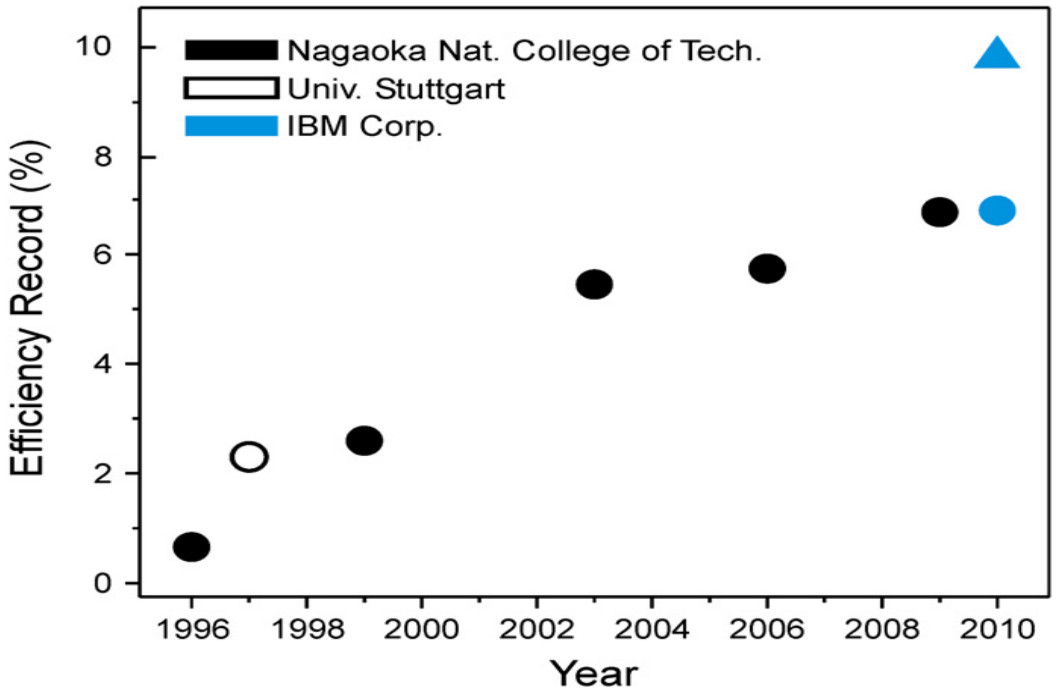


**Figure 1.3.** Record CZTSSe thin-film device performance vs. year, 1.6% (reported to be limited by a large series resistance), an open circuit voltage of 500 mV and a short circuit current density of 7.9 mA / $cm^2$.

By far the most extensive subsequent work on kesterite-related PV devices has been performed on CZTSSe materials, which are the primary focus of this review, leading to continual device performance improvement (Fig. 1.2) [41]. In 1996, Katagiri et al**.** [32, 41] reported on sequentially evaporated CTZS (pure sulfide) films, yielding a glass/Mo/CZTS/CdS/ZnO:Al device efficiency of 0.66% and open circuit voltage of 400 mV. Within a year, the Stuttgart University group had pushed the power conversion efficiency of a similarly prepared device to 2.3% [42]. Currently, the record power conversion efficiency for vacuum-deposited CZTS has improved to 6.8% [41]. For analogous selenide CZTSe devices, in 1997 Friedlmeier et al. [42] reported on vacuum-fabricated films, obtaining a device efficiency of 0.6%. By 2009 the efficiency for CZTSe devices had increased to 3.2% [35]. The current CZTSSe kesterite record of 9.7% (Fig. 1.2) was achieved using a hydrazine based solution deposition approach with mixed sulfur/selenium anions [30].

### 1.3 Aim of Thesis

Therefore, the semiconductor material $Cu_2ZnSnS_4$ need to be synthesized by some low cost techniques and its application for the solar cell should be studied. Hence, the work carried out in present thesis is aimed at the following points:

(i) To synthesize CZTS by low cost hydrothermal and traditional route.

(ii) To structurally and optically characterized the synthesized CZTS material.

(iii) To apply these materials a solar cell with P3HT, PCBM, CdSe.

(iv) The particles were investigated by X-Ray and transmission electron microscopy.

(v) Chapter 1 shows introduction and basic of CZTS. Chapter 2 shows experimental details of hydrothermal and solvothermal routes. The work finishes with a short conclusion.

# CHAPTER -2

# EXPERIMENTAL PROCEDURE

## 2.1 Synthesis

The synthesize CZTS has been done by solvothermal and hydrothermal. Technique have been described in subsequent subsection.

### 2.1.1 Solvothermal

Solvothermal synthesis is a method of producing chemical compounds. It is very similar to the hydrothermal route (where the synthesis is conducted in a stainless steel autoclave), the only difference being that the precursor solution is usually not aqueous (however, this is not always the case in all literature uses of the expression). Using the solvothermal route gains one the benefits of both the sol-gel and hydrothermal routes. Thus solvothermal synthesis allows for the precise control over the size, shape distribution, and crystallinity of by changing certain experimental parameters, including reaction temperature, reaction time, solvent type, surfactant type, and precursor type.

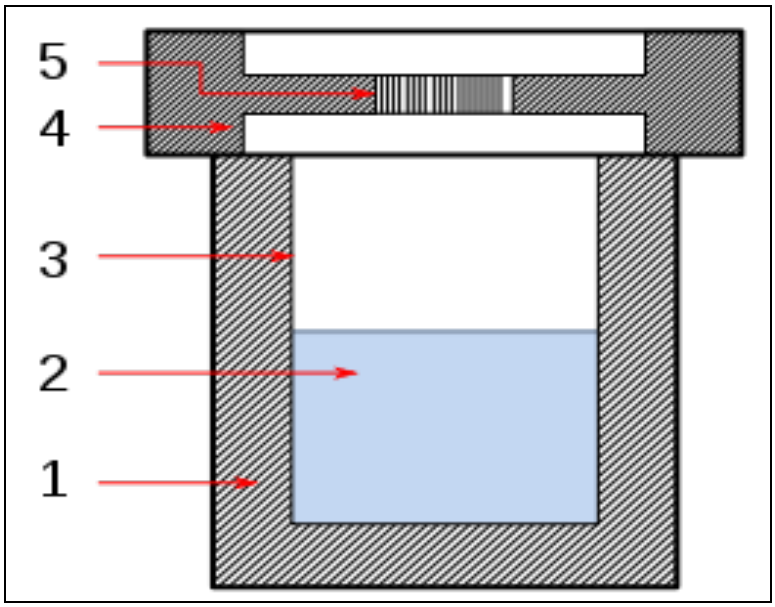


**Figure 2.0** Schematic diagram of solvothermal synthesis setup.

Figure 2.0 Shows schematic diagram of solvothermal synthesis setup: (1) stainless steel autoclave (2) precursor solution (3) Teflon liner (4) stainless steel lid (5) spring. Solvothermal synthesis has been used in laboratory to make nanostructured CZTS, titanium dioxide, graphene, carbon and other materials.

In a typical process, appropriate amounts of analytical grade $CuCl_2$, $(C_2H_3O_2)_2Zn$, $SnCl_4$ and S were added into a stainless steel autoclave with a Teflon liner, which was filled with ethylene diamine up to 50% of the total volume (1000mL). The auto clave was sealed and maintained at$180^0$C for15h and then allowed to cool to room temperature naturally. The precipitates were filtered off, washed with absolute ethanol. Finally, the products were collected for characterization.

### 2.1.2 Hydrothermal

Hydrothermal synthesis includes the various techniques of crystallizing substances from high-temperature aqueous solutions at high vapor pressures; also termed "hydrothermal method". The term "hydrothermal" is of geologic origin. Geochemists and mineralogists have studied hydrothermal phase equilibria since the beginning of the twentieth century. George W. Morey at the Carnegie Institution and later, Percy W. Bridgman at Harvard University did much of the work to lay the foundations necessary to containment of reactive media in the temperature and pressure range where most of the hydrothermal work is conducted.

Hydrothermal synthesis can be defined as a method of synthesis of single crystals that depends on the solubility of minerals in hot water under high pressure. The crystal growth is performed in an apparatus consisting of a steel pressure vessel called autoclave, in which a nutrient is supplied along with water. A gradient of temperature is maintained at the opposite ends of the growth chamber so that the hotter end dissolves the nutrient and the cooler end causes seeds to take additional growth.

Possible advantages of the hydrothermal method over other types of crystal growth include the ability to create crystalline phases which are not stable at the melting point. Also, materials which have a high vapour pressure near their melting points can

also be grown by the hydrothermal method. The method is also particularly suitable for the growth of large good-quality crystals while maintaining good control over their composition. Disadvantages of the method include the need of expensive autoclaves, and the impossibility of observing the crystal as it grows [48].

**Equipment for hydrothermal crystal growth**

The crystallization vessels used are autoclaves. These are usually thick-walled steel cylinders with a hermetic seal which must withstand high temperatures and pressures for prolonged periods of time. Furthermore, the autoclave material must be inert with respect to the solvent. The closure is the most important element of the autoclave. Many designs have been developed for seals, the most famous being the Bridgman seal. In most cases steel-corroding solutions are used in hydrothermal experiments. To prevent corrosion of the internal cavity of the autoclave, protective inserts are generally used. These may have the same shape of the autoclave and fit in the internal cavity (contact-type insert) or be a "floating" type insert which occupies only part of the autoclave interior. Inserts may be made of carbon-free iron, copper, silver, gold, platinum, titanium, glass (or quartz), or Teflon, depending on the temperature and solution used.

In a typical process, appropriate amounts of analytical grade $CuCl_2$, $(C_2H_3O_2)_2Zn$, $SnCl_4$ and S were added into a stainless steel autoclave with a Teflon liner, which was filled with double distilled water up to 50% of the total volume (1000mL). The auto clave was sealed and maintained at$180^0$C for15h and then allowed to cool to room temperature naturally. The precipitates were filtered off, washed with absolute ethanol. Finally, the products were collected for characterization.

**2.1.3 Hydrothermal at Nitrogen atmosphere**

In a typical process, appropriate amounts of analytical grade $CuCl_2$, $(C_2H_3O_2)_2Zn$, $SnCl_4$ and thiourea were added into a stainless steel autoclave with a Teflon liner, which was filled with double distilled water up to 50% of the total volume (1000mL). The auto clave was purging by nitrogen gas three times after this sealed and

maintained at180$^0$C for15h and then allowed to cool to room temperature naturally. The precipitates were filtered off, washed with double distilled water. Finally, the products were collected for characterization. Same process applies for 200$^0$C and 160$^0$C for 15h and then allows cooling to room temperature naturally, open autoclave wash and filtered off. Finally, the products were collected for characterization.

**Equipment**

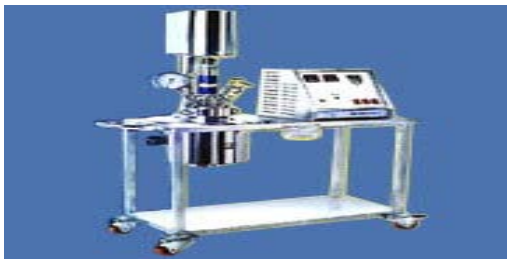

**Figure 2.1** High Pressure Laboratory Autoclaves at NPL,Delhi

### 2.1.4 Reactants and other used Reagents

Cupric chloride di hydrate, $CuCl_2.2H_2O$

S.d fine-chem Limited 99% A.R., M.W. 170.48 g mol$^{-1}$

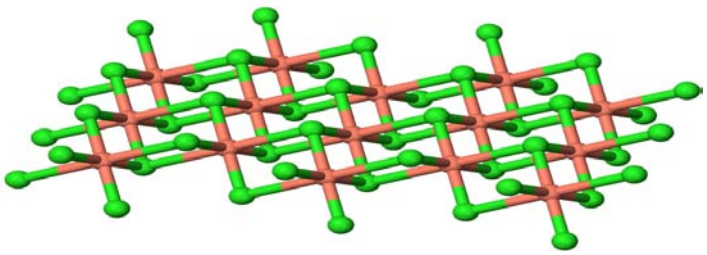

**Figure.2.2** Chemical structure of cupric chloride dehydrate

Stannic Chloride Pent hydrate, $SnCl_4.5H_2O$

Central Drug House (CDH) 97.5% A.R. M.W. 350.58 g mol$^{-1}$

Zinc acetate $(CH3.COO)_2$ $Zn.2H_2O$

Central Drug House (CDH), 99.5% A.R. M.W. 219.50 g $mol^{-1}$

Thiourea ($H_2NCSNH_2$)

Aldrich Chemical Company, 99% L.R. M.W.76.12 g $mol^{-1}$

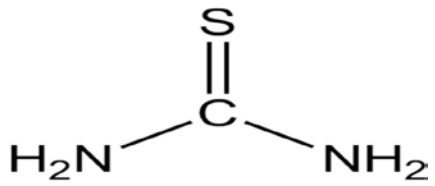


**Figure 2.3** Chemical structure of thiourea

## 2.2 X-ray – Spectroscopy

With X-ray-diffraction it is possible to identify the distances of the crystal lattice planes. Therefore it is possible to analyze substances qualitatively and quantitatively. In this thesis X-ray-diffraction was used to identify Cu2ZnSnS4 qualitatively. The measuring principle is based on the reflection, respectively diffraction of X-ray. To generate monochromatic X-ray a β-filter (in case of CuKα, a nickel-filter) is used. It filters the brems spectrum and all the other not used X-Ray lines out from the emitted spectrum of the X-ray source (in the majority of cases a copper anode). If one of this monochromatic X-ray hits the sample, parts of the X-ray will be absorbed and others will be reflected, respectively diffracted. Due to the diffraction the overlapping of waves happens. Depending on the geometrical orientation the overlapping leads to amplification or erasement. If the Bragg Equation (Equation 1) is fulfilled a maximum of the intensity is detected with the counter. In Figure 2.4 a schematic configuration of a conventional X-ray diffraction machine can be seen. The X-ray hits the sample under an adjustable angle $\theta$. The intensity of the reflected beam is measured with the detector. The detector moves

with a variating glancing angle $\theta$ on the measuring circuit in the way that the angle between the beam direction and the detector is always 2θ.

**Bragg Equation:**

X-ray-reflexes can only be detected if any lattice plane with the Miller indices (*h k l*) fulfills the Bragg equation [15]:

Equation 1:

$$n * \lambda = 2 * d_{hkl} * \sin \Theta$$

*n*…..order

$\lambda$…..wavelength of Cu-Kα-radiation

$d_{hkl}$…..distance between two lattice planes

$\theta$…..used glancing angle

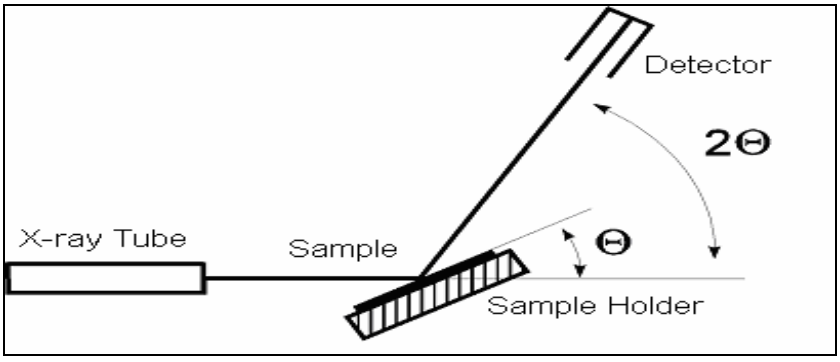


**Figure 2.4**: Configuration of X-ray diffraction machine [33]

The measured spectra show maxima of intensity at certain angles. The phases inside the sample can be identified and the maxima can be assigned, by comparing the spectra to references from the JCPDS data and with theoretically calculated diffract grams.

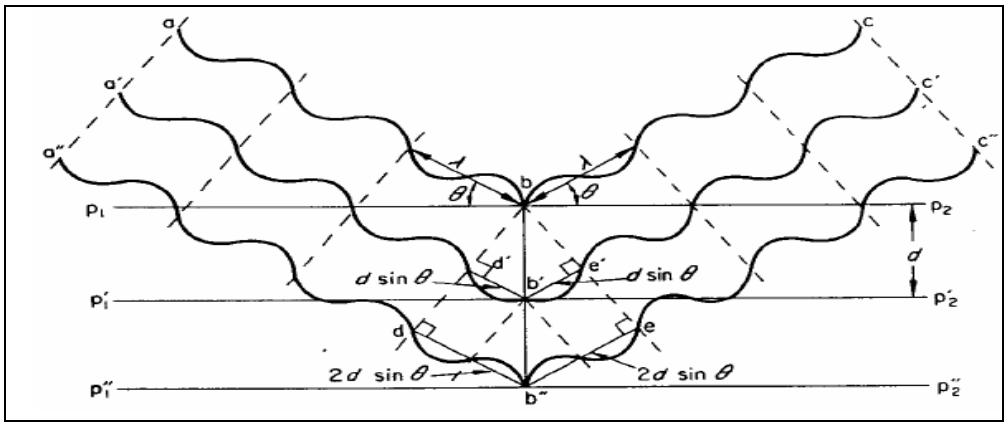


Figure 2.5: Condition for diffraction of X-ray radiation

.

## 2.3 Transmission Electron Microscopy Measurements

A Transmission Electron Microscope (TEM) (Jeol 2012 F. as TEM, Jeol, Tokio, J) was used to estimate the size of the particles. The solution of $Cu_2ZnSnS_4$ in ethanol (Like after the synthesis: 0.05 mol l-1) was dropped on a copper-grate and dried for two hours under air. Afterwards they were dried at 80 °C in the vacuum oven over Night. In Figure 1.6 the configuration of a TEM is shown. The virtual source at the top is an electron gun. It produces a stream of monochromatic electrons. The stream is focused to a small, thin, coherent beam by the use of the magnetic condenser lenses 1 and 2. The first lens determines the general size range of the final spot that strikes the sample. The second lens changes the size of the spot on the sample from a wide disperse spot to a pinpoint beam. The beam is restricted by the condenser aperture, knocking out high angle electrons. Next the beam strikes the sample and parts of it are transmitted. An objective lens focuses the transition portion into an image. Optional objective and selected area metal apertures can restrict the beam; the object aperture enhancing contrast by blocking high-angle diffracted electrons; the selected area aperture enables the user to examine the periodic diffraction of electrons by ordered arrangements of atoms in the sample.

Through the intermediate and projector lenses the image is passed down through the column, being enlarged all the way. The image strikes the phosphor image screen and light is generated, so the user can see the image. [45]

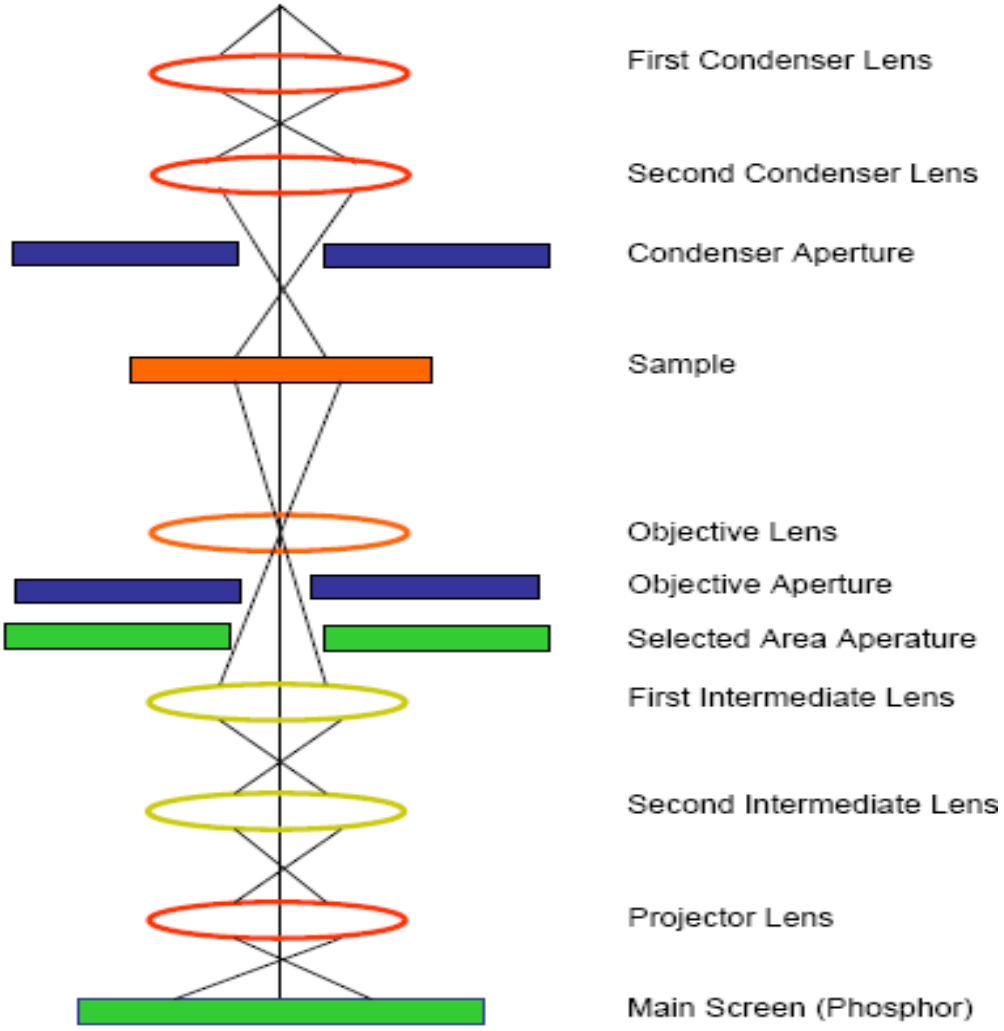


**Figure 2.6:** Configuration of a Transmission Electron Microscope

## 2.4 Ultraviolet and Visible (UV-Vis) Absorption Spectroscopy

The word 'spectroscopy' is used as a collective term for all the analytical techniques based on the interaction of light and matter. Spectro photometry is one of the

branches of spectroscopy where we measure the absorption of light by molecules that are in a gas or vapour state or dissolved molecules/ions. Spectro-photometry investigates the absorption of the different substances between the wavelength limits 190 nm and 780 nm (visible spectroscopy is restricted to the wavelength range of electromagnetic radiation detectable by the human eye, that is above ~360 nm; ultraviolet spectroscopy is used for shorter wavelengths). In this wavelength range the absorption of the electromagnetic radiation is caused by the excitation (i.e. transition to a higher energy level) of the bonding and non-bonding electrons of the ions or molecules. A graph of absorbance against wavelength gives the sample's absorption spectrum. Modern spectrophotometers draw this automatically. The measured spectrum is continuous, due to the fact that the different vibration and rotation states of the molecules make the absorption band wider.

Spectrophotometry is used for both qualitative and quantitative investigations of samples. The wavelength at the maximum of the absorption band will give information about the structure of the molecule or ion and the extent of the absorption is proportional with the amount of the species absorbing the light. Quantitative measurements are based on Beer's Law (also known as "Lambert- Beer Law" or even "Bouguer-Lambert-Beer Law") which is described as follows:

$$A = e\ c\ l$$

Where $A$ = absorbance [no units, because it is calculated as $A = \log10\ (I_0/I)$, where $I_0$ is the incident light's intensity and $I$ is the light intensity after it passes through the sample];
$e$ = molar absorbance or absorption coefficient [in $dm^3\ mol^{-1}\ cm^{-1}$ units];
$c$ = concentration (molarity) of the compound in the solution [in mol $dm^{-3}$units];
$l$ = path length of light in the sample [in cm units].

The instruments used for spectro photometry are called photometers and spectrophotometers (fig. 2.7). The difference between them is that we can only make measurements at a particular wavelength with a photometer, but spectrophotometers can be used for the whole wavelength range. [46]

Both types of instruments have suitable light sources, monochromator (that selects the light with the necessary wavelength) and a detector. The solution is put into a sample tube (called a “cuvette”). The light intensity measured by the detector is converted into an electric signal and is displayed as a certain absorbance on the readout (fig. 2.8.).

**Figure 2.7**: Photograph of a spectrophotometer

The quantitative determinations made by spectrophotometry could be divided in two groups according to the number of substances to be measured. These are the analytical measurements of systems that consist of only one absorbing component and systems that consist of more than one absorbing component. In the case of systems containing one absorbing component we measure the absorption of light at a particular wavelength (which is usually identical with the absorption maximum of the analyte). We either calculate the concentration from the results by using the molar absorptivity found

in the literature or the unknown concentration can be determined by comparing the results with a working curve of absorbance versus concentration (calibration curve) derived using standards. [47]

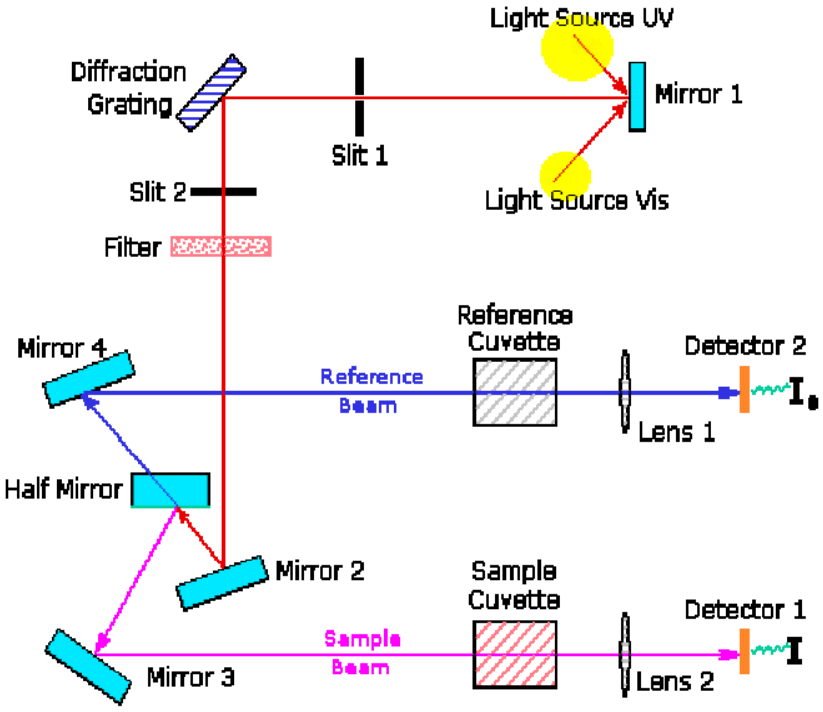


**Figure 2.8**: Principle of UV/Vis spectrometer

## 2.5 Device Preparation

For the solar cells different structures were used:

### 2.5.1 Solar Cell Schemata

For bilayer solar cells two different structures were used: The first structure can be seen in Figure 2.9 (i). A CZTS layer was spin coated on ITO covered glass, then a layer of PCBM was drop casted and the electrodes (Al) were evaporated on top. The

other structure is shown in Figure 1.9 (ii). A layer of CZTS was spin coated on ITO coverd glass and then a layer of P3HT was drop casted on top, on this layer the Al electrodes were evaporated.


(i) (ii)

**Figure 2.9:** Scheme of a bilayer solar cell: ITO covered glass / CZTS layer (i) drop cast PCBM (ii) Drop cast $P_3HT$ layer /evaporated top electrode (Al).

### 2.5.2 Substrate Preparation

#### ITO Coated Glass

Indium – tin – oxide (ITO) coated glass sheets were cut into 1.5 cm x 1.5 cm substrates for Spin coating or drop casting, and to 1.5 cm x 4.5 cm substrates for dip coating. To prevent short circuits one third of the ITO surface was removed with strong acid (HClconc.: $H_2O$ = 3: 1). The strip wise rest of the surface was protected against the acid by a tape. Wash it 4 to 6 times with Zn dust and hydrogen released. After 30 min. acid wash with running water. The substrates were now cleaned each for 15 minutes three times with acetone and once with isopropanol in an ultrasonic bath. Sample boil with trichloroethylene (TCE), pull out with the help of twizer and put in the petridish.

### 2.5.3 PCBM Layer in Bilayer Solar Cells

The systematic name of PCBM is 1 - (3 - methoxycarbonyl) propyl – 1 – phenyl [6, 6] $C_{61}$. It is a derivate of a Buckminsterfullerene and the side chain changes the properties. Therefore PCBM is soluble in organic solvents like chloroform, dichlorobenzene, chlorobenzene or toluene. The chemical structure of PCBM can be seen in Figure 3.0. It was used as electron acceptor.

PCBM was drop cast (20 mg/ml) or spins coated (1500 rpm, 40 s) from 3 wt % solutions

in chlorbenzene. The devices were dried under non vacuum for 45 minutes at $60^0$C.

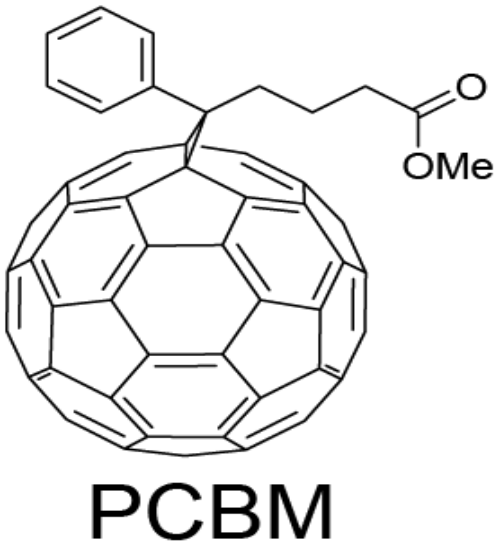


**Figure 3.0:** Chemical Structure of PCBM

The systematic name of P3HT is Poly (3 - hexylthiophene - 2,2 - diyl). The chemical structure can be seen in Figure 2.0. It is highly soluble in common organic solvents. The P3HT and PCBM Was purchased from USA (Aldrich Chemicals).

P3HT was spin coated (1500 rpm, 40 s) or drop cast (20 mg / ml) from solutions in chlorobenzene or chloroform. The devices were dried under non vacuum for 45 minutes at $60^0$C.

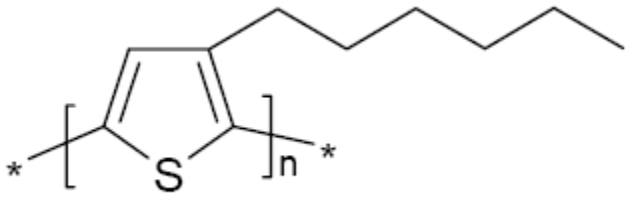


**Figure 3.1:** Chemical Structure of P3HT

### 2.5.4 PEDOT: PSS Layers

PEDOT: PSS layers were used for cells with geometry as shown in Figure 2.2. PEDOT: PSS is a mixture of poly (3, 4 – ethylene di oxy thio phene) and poly (styrene sulfonate). It was purchased (Aldrich Chemicals, 1.3 wt% dispersion in water) from USA. The aqueous dispersion (particle size of 80 nm, 0.5 w% PEDOT: PSS = 2 : 3) was spin coated twice on the ITO substrate (1500 rpm, 40 s) and dried for 1h at120$^0$C night under vacuum. PEDOT: PSS is used as an interfacial hole conducting and electron blocking layer.

Figure 3.2 shows the chemical structure:

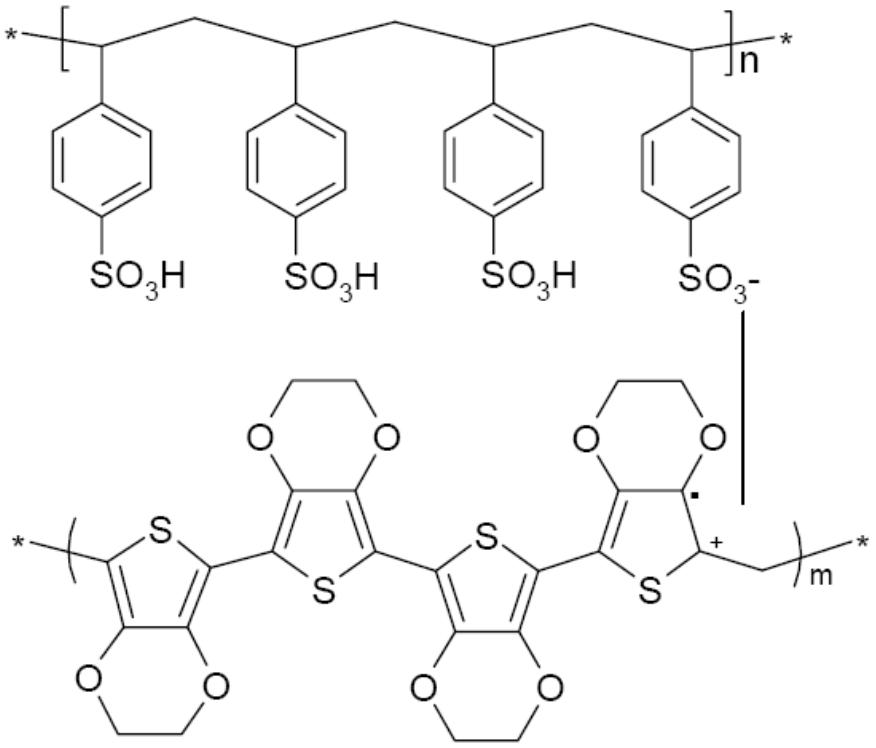


Figure 3.2: Chemical structure of electrochemical doped PEDOT: PSS

### 2.5.5 Top Contact Evaporation

After the active layers were applied the top contacts were thermally evaporated under high vacuum (approximately 1 * 10-5 mbar) in a Leybold evaporation chamber (Leybold Vacuum, Cologne, Germany). The metals for the evaporation were placed into a molybednum boat. The evaporation rate (0.005 nm / s for LiF, 0.01 increasing to 0.1 nm / s for Al and 0.1 nm / s for Au) was monitored by a quartz balance, Intellemetrics IC 600. The evaporation was done through a shadow mask. 0.6 nm of LiF were followed by 80 nm of Al. The interfacial layer of LiF is known to improve the electron exitation, respectively injection [54] and also an increase in fill factors and a stabilization of high Voc´s are observed [55]. For the cells with Au as top contact 80 nm were evaporated except for the CISCuT-cells: only 5 nm of Au were evaporated because the contact has to be semitransparent.

## 2.6 Current-Voltage Measurements

These measurements were done in normal atmosphere. A Streunagel solar simulator (with metal halogen lamp as light source and with an AM 1.5 filter) was used. For the measurements the intensity was calibrated to 100 mW $cm^{-2}$. The $J - V$ curves were measured with a Keithley 2400 (Keithley Instruments, Inc., Cleveland, Ohio; USA) sweeping from – 1 V to + 1V. The electrodes were ITO and Al or Au. $J - V$ curves give important parameters to describe a solar cell. These parameters are: The open-circuit voltage ($V_{OC}$), the short-circuit current ($j_{SC}$) and the maximum-power-point (mpp). The mmp is defined as the point inside the fourth quadrant where the product of $J$ times $V$ has a maximum. It defines the maximum power voltage ($V$mpp) and the maximum–power current ($j_{mpp}$). This can be seen in Figure 21. Another important parameter for solar cells is the fill factor ($FF$). It describes the quality of the diode:

**Equation 2**

$$FF = \frac{V_{mpp} * j_{mpp}}{V_{OC} * j_{SC}}$$

For an ideal diode *FF* approaches 1. With the *FF* the efficiency can be calculated

**Equation 3**

$$\eta_{AM1.5} = \frac{j_{SC} * V_{OC} * FF}{P_{light}}$$

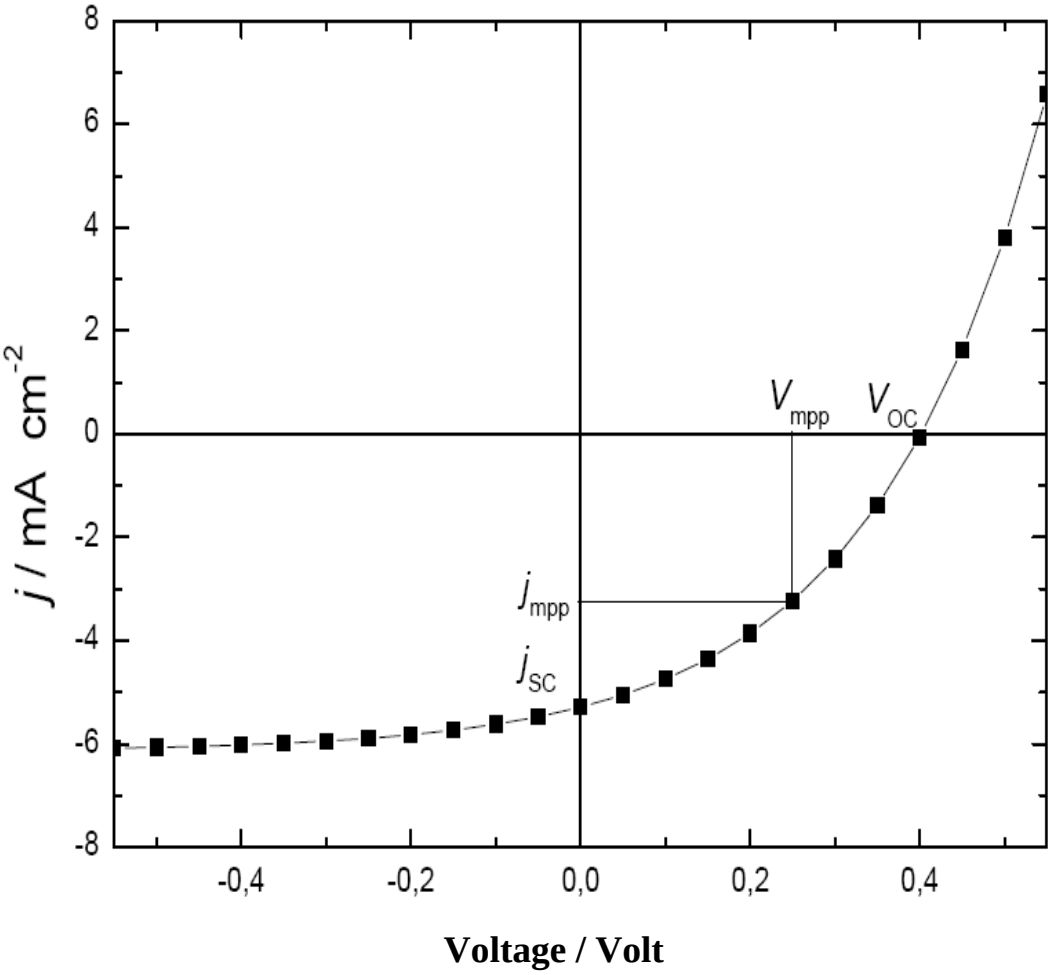


**Figure 3.3:** Definition of $V_{OC}$ , $j_{sc}$ , $V_{mpp}$, $j_{mpp}$

# CHAPTER 3

# RESULT AND DISCUSSION

## 3.1Characterization:

The synthesized sample of CZTS has been structurally and optically characterized for determining the phase purity, surface morphology, particle size and band gap of the material.

### 3.1 .1 Structural:

The structure of the sample has been carried out by using XRD, SEM, TEM. The details are given below.

#### 3.1.1.1 XRD:

Fig.3.1.1 shows the XRD patterns of the as synthesized CZTS nanoparticles, the peaks appeared at 2θ=28.55, 33.04, 47.56, 56.25, 69.34 and 76.34 can be attributed to the diffraction of (112),(200),(220),(303),(008) and (332) orientation of kesterite structure of CZTS (JCPDS 26-0575). Kesterite has a tetragonal unit cell inside which sulphur anion layers along the crystallographic c-direction as CuZn/SS/CuSn/SS [43]. Beside these, the peaks appeared at 2θ=26.91, 39.61, and 51.77 can be attributed to the diffraction of (100), (102) and (103) orientation of wurtzite-2H structure of ZnS (JCPDS 36-1450). No direct information could be found to confirm the existence of SnS or $SnS_2$. High temperature treatment could increase the crystalline and grain size of CZTS films, which conduces to fabricate high efficiency solar cell because the efficiency of After being annealed at $350^0$C for1h under nitrogen gas, the crystalline and the purity of CZTS nanoparticles were greatly improved, as indicated in Figure (3.3). With the strongest diffraction peak of the (112) plane ,according to the Debye–Scherrer formula: $D=0.89\lambda/(B\cos(\theta))$ (λ is the incident X-ray wavelength, B the full-width at half-maximum (FWHM) of diffraction

peak, θ the diffraction angle),the diameters D of as-synthesized and annealed CZTS nanoparticle were evaluated to be 4.95 and 32.42 nm, respectively.

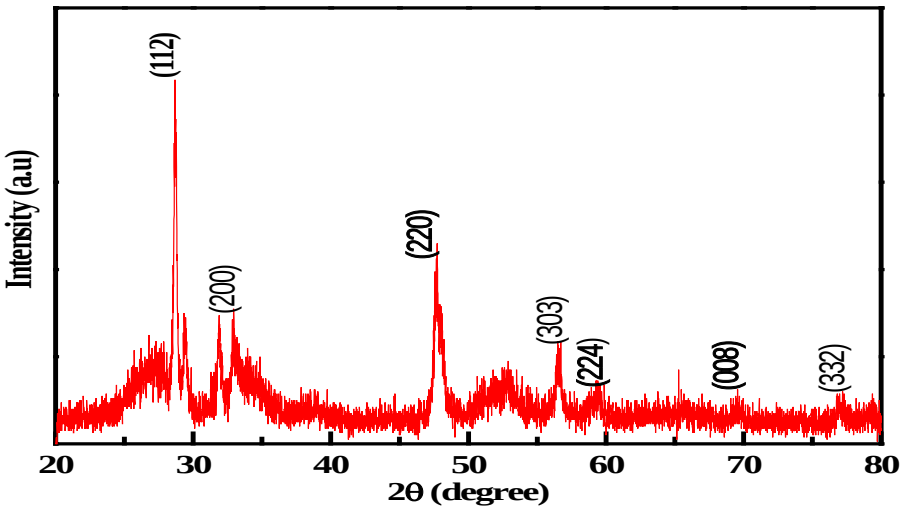


Figure 3.1.1 Shows Xrd of Hydrothermal CZTS.

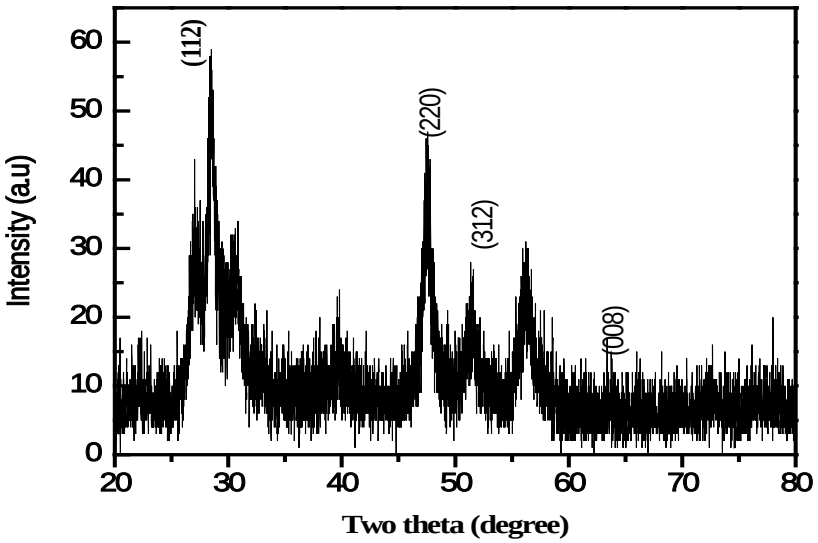


Figure 3.1.2 Shows Xrd of Solvothermal CZTS

High-temperature treatment could increase the crystallinity and grain size of CZTS films, which conduces to fabricate high efficiency solar cell because the efficiency of poly-crystalline solar cell increases with an increase in grain size of the absorbed layer

material [49]. Figure 3.4.1 shows Xrd of three different temperatures. All three Xrd are match with each other.

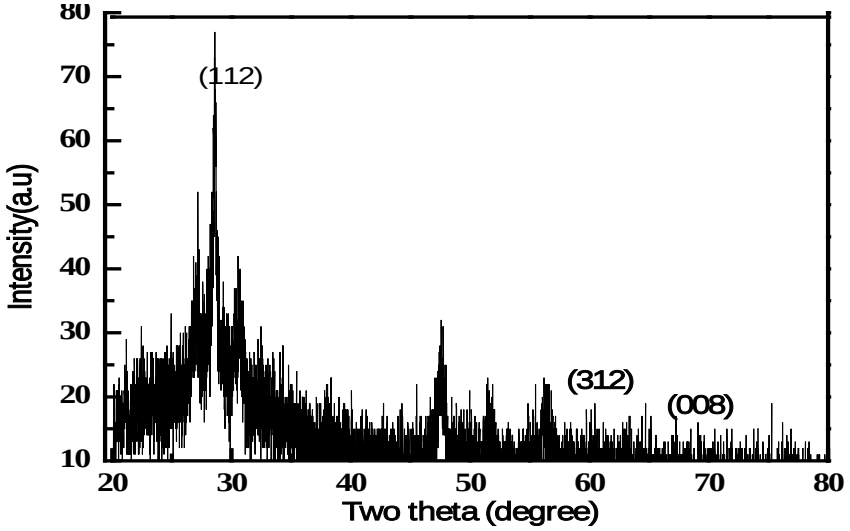


Figure 3.1.3 Shows Xrd of Solvothermal CZTS annealed at $350^0$C with Nitrogen atmosphere.

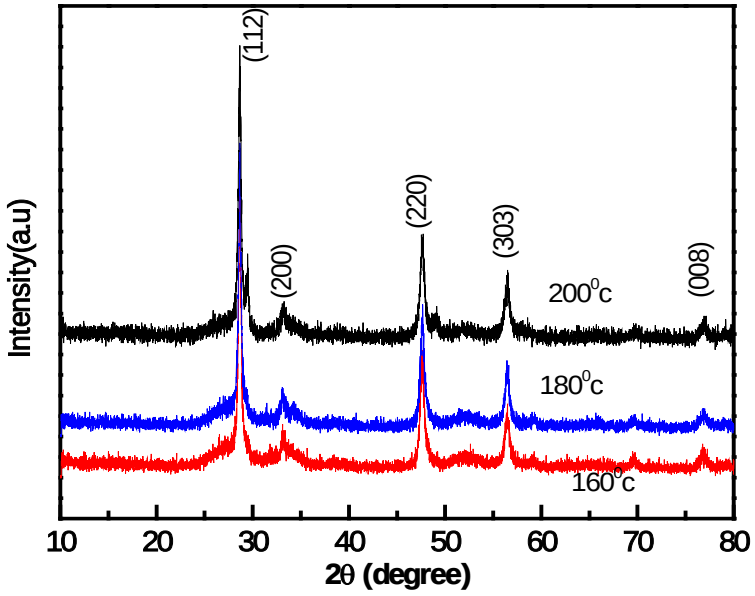


**Figure 3**.4.1 Shows XRD at different temperatures

### 3.1.1.2 SEM

Fig. 3.5.1 is the SEM image of the CZTS nanoparticle coated on to the conductive carbon tape with holder at different magnification. A continuous film with large grains was formed from aggregation of small CZTS nanoparticles on the conductive carbon tape. But cracks existed in the films, which are not beneficial to photovoltaic application [56].

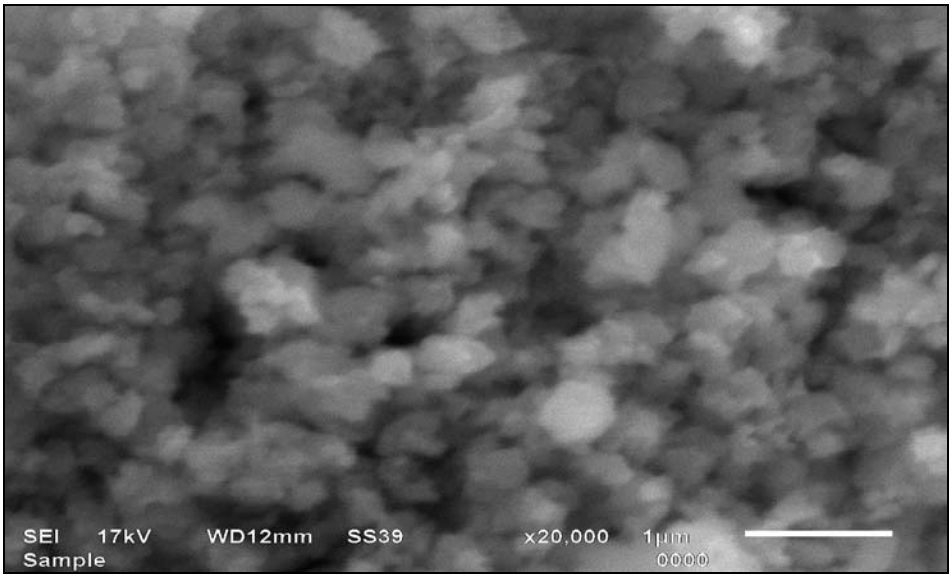


**Figure 3.5.1** SEM images (X20, 000) of Hydrothermal CZTS Shows Surface morphology its grain size around 0.38 micrometer.

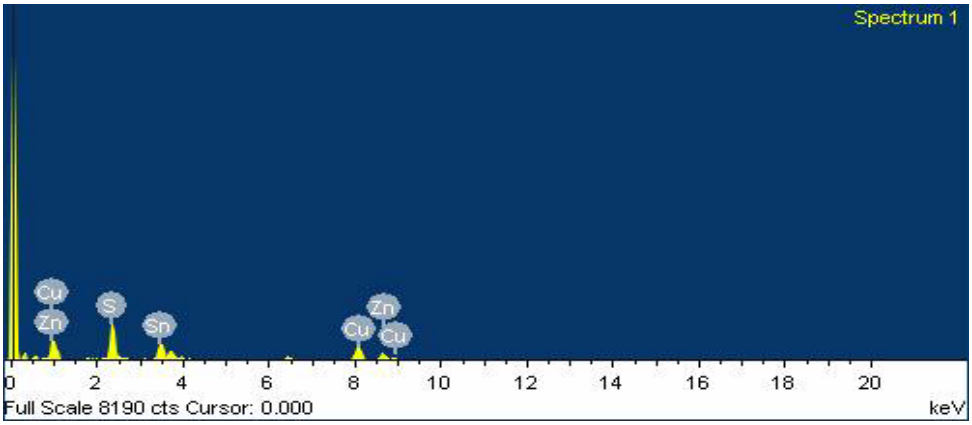


**Figure 3.6.1** Shows EDX

Conductive Carbon tape with binder addition spread nanoparticles of CZTS may be crack free relatively, but it needs further study. Fig. 3.6.1 shows are presentative EDX pattern of CZTS nanoparticle thin films in conductive carbon tape. The chemical composition ratios of CZTS nanoparticle thin films are Cu:Zn:Sn:S=32:21:13:34.The observed chemical composition from EDAX is near to the theoretical chemical composition of CZTS. Usually, chemical composition of sulfides shows deficiency of S [50]. Our as-synthesised nanoparticles are slightly tin rich only because of the excess of $SnCl_4$ before reaction, but the composition is within the range of compositions reported for CZTS films by several researchers [51].

| Element | Weight% | Atomic% |
|---|---|---|
| S K | 17.71 | 33.60 |
| Cu K | 33.48 | 32.06 |
| Zn K | 22.27 | 20.73 |
| Sn K | 26.53 | 13.60 |
| Totals | 100.00 | 100.00 |

**Table 2.** Shows Composition of CZTS in EDX image

## Grain size

It is often very difficult to determine the grain size from SEM images. Main problem is that the cross section does not show an even fracture plane, but a very square-edged side. It is often impossible to determine where grains begin and where they end, or whether several grains "overlap" in the image but appear as one; a general topographical problem when a three-dimensional structure is pictured in a two-dimensional image. Another problem is that it sometimes was not possible to get a sufficient contrast for the images (see for example Fig. 3.5&3.7) due to charging effects, which made it nearly impossible to estimate grain size.

However, for most samples an impression could be received if the grains appear ’larger’, by which we mean here clearly bigger than 0.38 μm, or smaller (less than 0.5 μm). In these categories, no clear trend for grain sizes related to composition could be found.

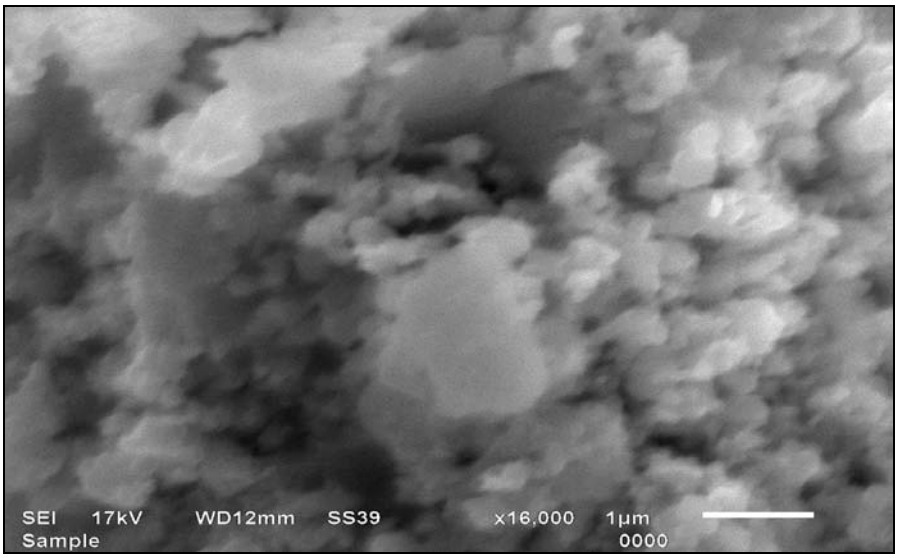


**Figure 3.7** SEM image at X16, 000 of Hydrothermal CZTS Shows Surface morphology.

### 3.1.1.3 TEM

Figure.3.8&3.9 shows a TEM image of the as-synthesised CZTS nanoparticles with particle sizes about 4-8 nm by hydrothermal and 5-10 nm by Solvothermal. High-resolution (5nm) TEM in figure 3.8 (a) shows that the nanoparticle is single-crystalline and the inter planar spacing of $3.1^{0}$A or 0.31nm corresponding to the (112) plane of CZTS nanoparticles and same inter planar distance in image 4.0 corresponding to (112). The CZTS nanoparticle are slightly dispersed, and how to enhance their dispersibility still needs further study. Fig.3.9b and 4.0b The selected area electron diffraction (SAED) pattern in matches the structure of CZTS, as indicated by the diffraction spots corresponding to the (112), (200) and (312) planes in both 3.8 and 3.9 figure.

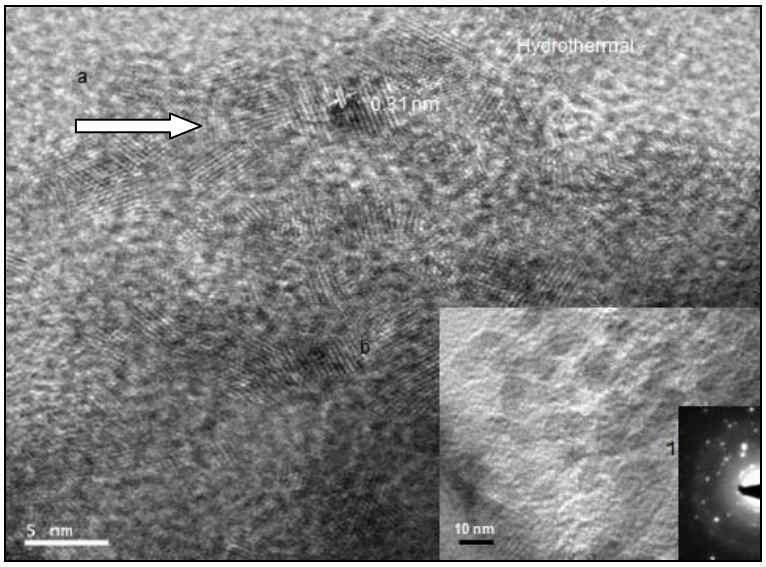


**Figure 3.8** Shows TEM image of Hydrothermal (a) and high-resolution TEM Characterizations of as-synthesized (b) Low resolution TEM (c) CZTS nanoparticles. The SAED pattern in the inset of was indexed to CZTS.

.

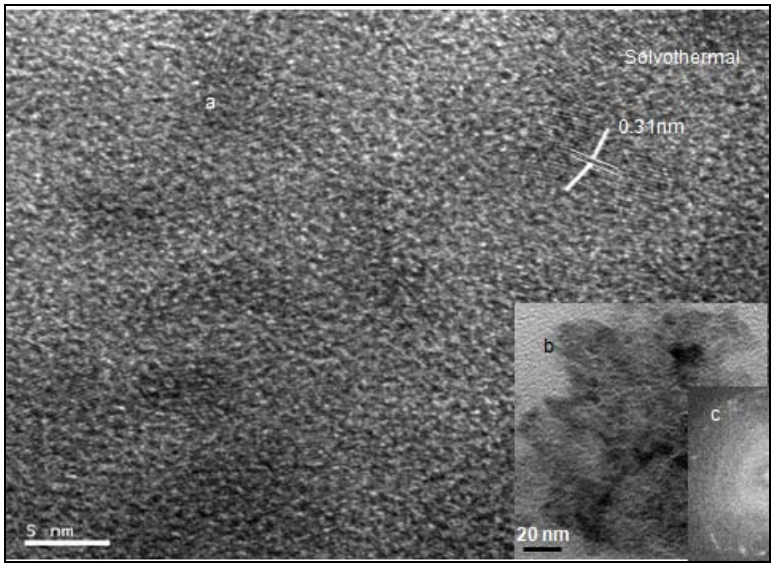


**Figure 3.9** TEM image of solvothermal (a) and high-resolution TEM Characterizations of as-synthesized (b) Low resolution TEM. (c) CZTS nanoparticles. The SAED pattern in the inset of was indexed to CZTS

## 3.2 Optical Characterizations:

Optical characterization has been done for band gap of semiconductor material CZTS. This has been done by employing UV visible spectroscopy and photo luminance spectroscopy. The details are given below.

### 3.2.1 UV visible

Figure 3.2.1&3.2.2 shows the UV–vis absorption spectroscopy of the CZTS nanoparticles. The energy band structure of CZTS has already been calculated and the measured gap of kesterite CZTS is Eg 1.05–1.55 eV [12, 13]. Figure 3.2.4 shows hydrothermally as synthesized nanoparticle. This nanoparticle contains 1.5eV bandgap .These result are taken without nitrogen atmosphere. Figure 3.2.3 shows high absorption at different temperature with nitrogen atmosphere. In the present study, the band gap was calculated to be about1.5eV by plotting $(\alpha h\nu)^2$ vs. hν in the absorption spectroscopy, where a is the absorption coefficient and hν is the photo-energy. Figure.3.2.6 shows different band gap with temperature. If we decreases or increases temperature in comparison of $180^0$C. Its band gap decreases. As shown in figure. At $180^0$C,$200^0$C,$160^0$C with nitrogen atmosphere synthesized nanoparticles band gap 1.45, 1.1.1.05eV.This value corresponds well with the literature values and is near the optimum value for photovoltaic solar conversion in a single-band-gap device. But at $180^0$C synthesized nanoparticles are best for photovoltaic solar conversion.

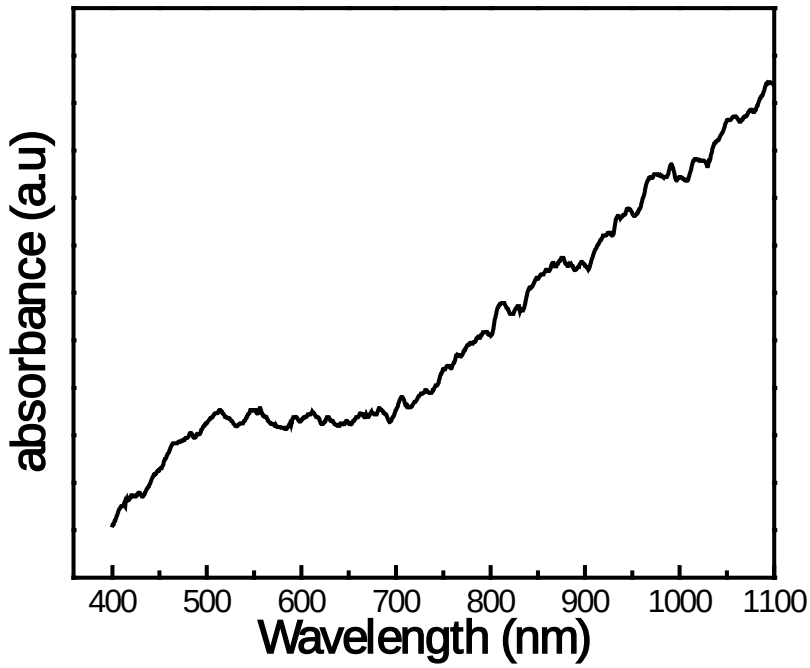


**Figure3.2.1** Shows absorbance of hydrothermal

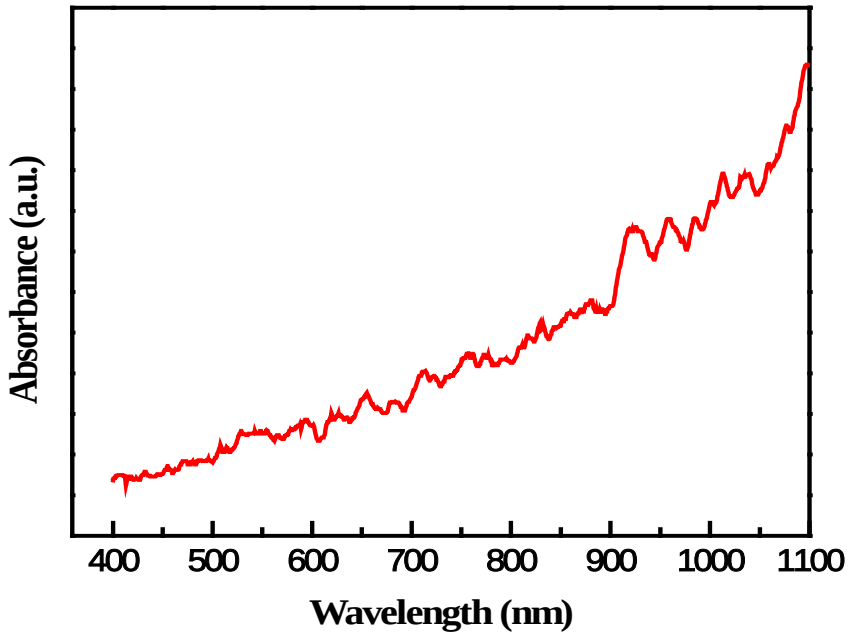


**Figure 3.2.2** Absorbance of solvothermal

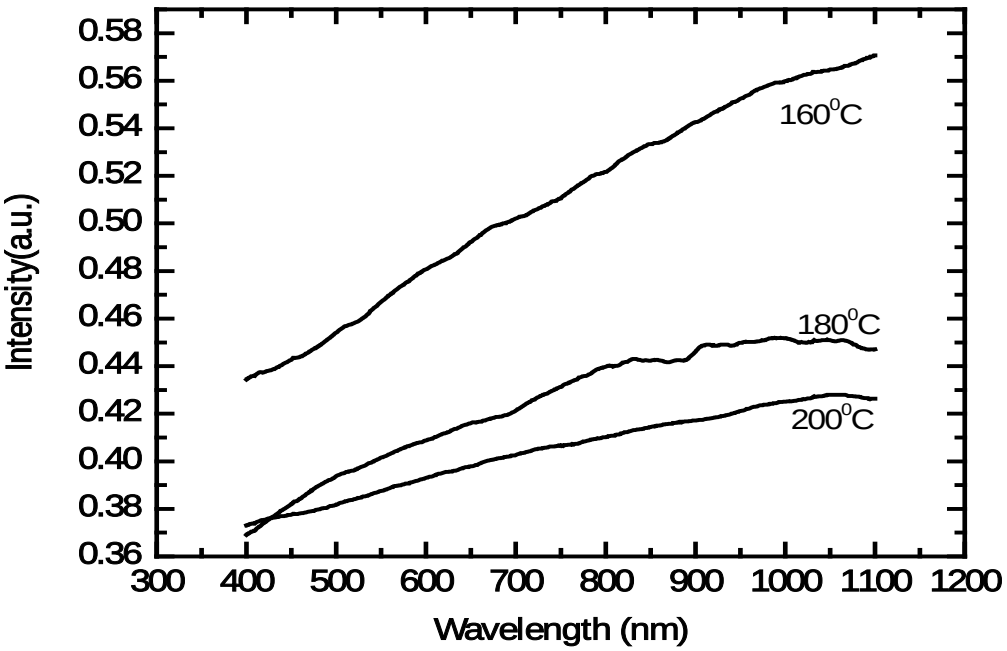


**Figure 3.2.3** Shows absorbance of Hydrothermal with nitrogen at $200^0$C,$180^0$C,$160^0$C

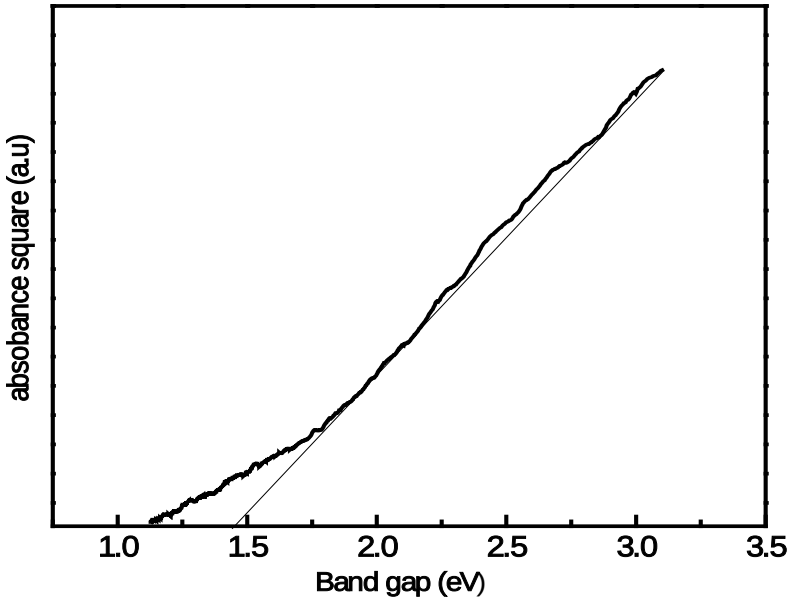


**Figure 3.2.4.**Shows band gap of hydrothermal without nitrogen

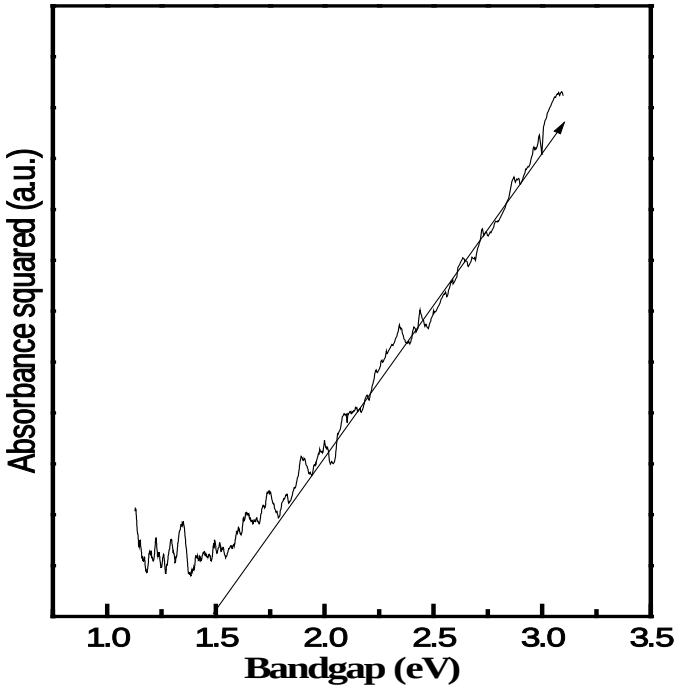


**Figure 3.2.5** Shows Band gap of Solvothermal without nitrogen

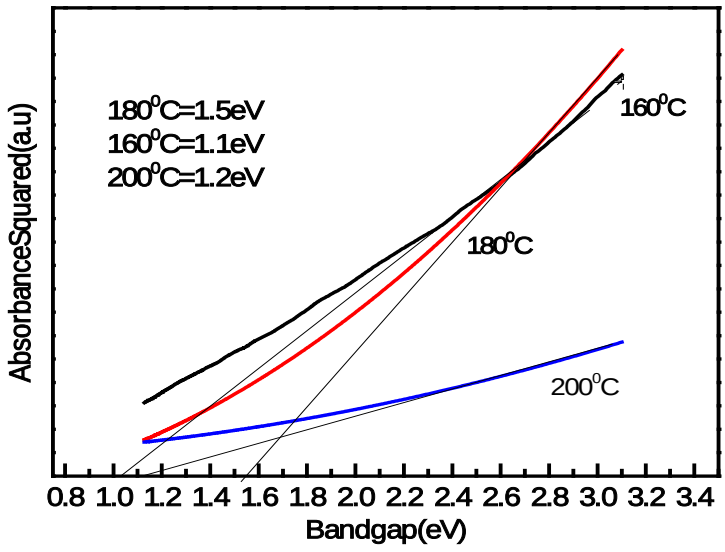


**Figure.3.2.6** Shows the band gap at different temperature of semiconductor Material**.**

### 3.3 Electrical Characterizations

Electrical characterization has been done by Keithley instrument and results are shown below in the graph.

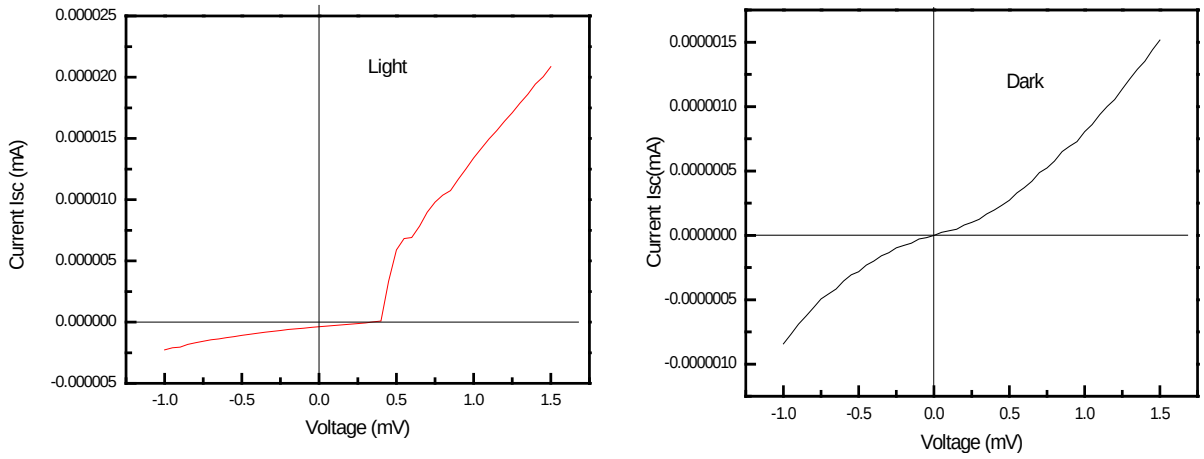


Figure 3.3.1 shows light and Dark ITO/P3HT/CZTS/Al

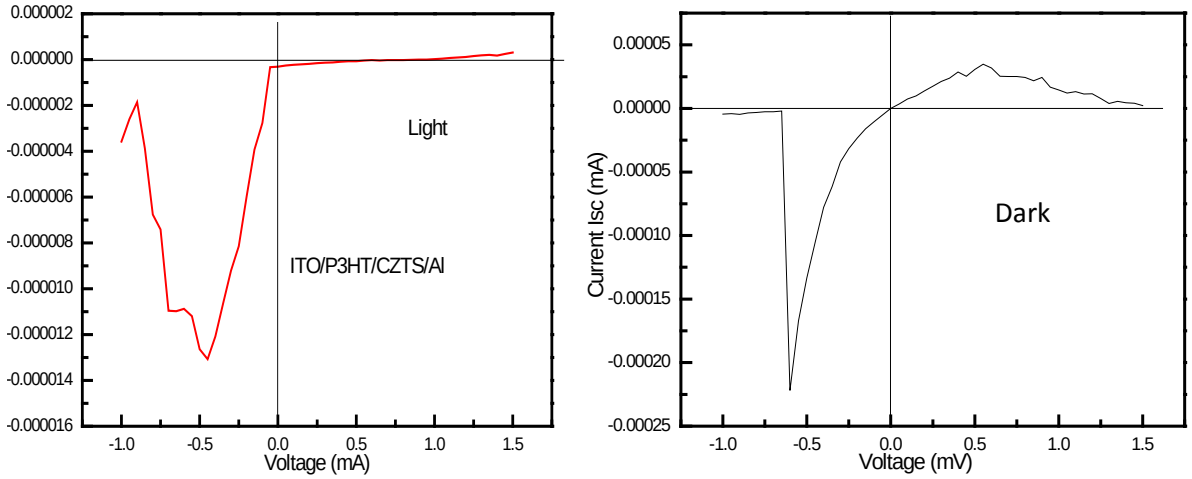


Figure 3.3.1 shows light and Dark ITO/P3HT/CZTS/Al

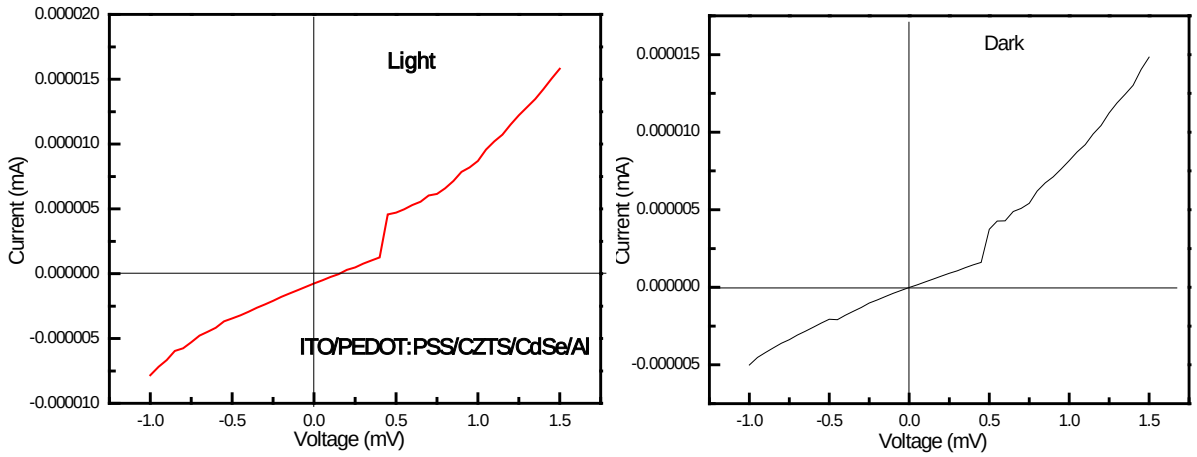


Figure 3.3.2 shows light and Dark ITO/PEDOT: PSS/CZTS/CdSe/Al

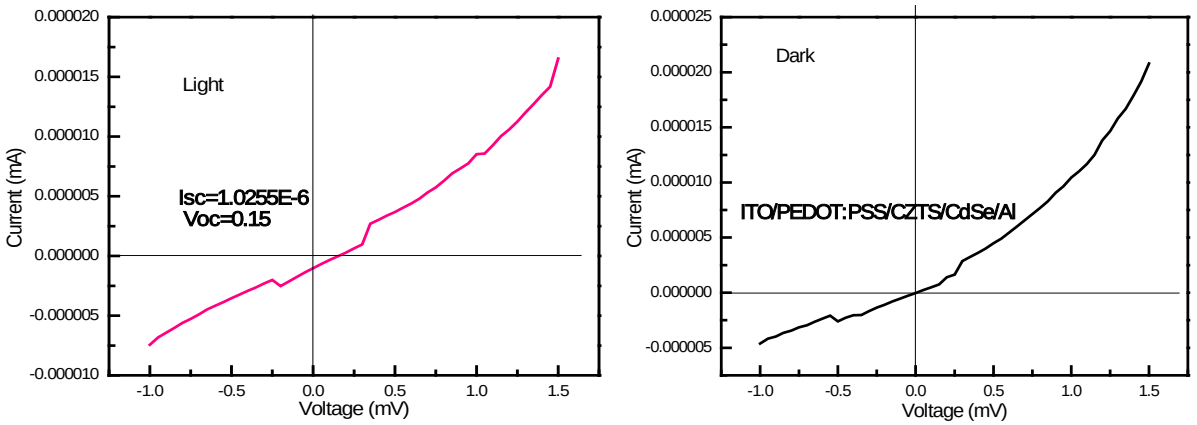


Figure 3.3.3 shows light and Dark ITO/PEDOT: PSS/CZTS/CdSe/Al

These IV characteristics are taken in the room temperature with the help of Keithely 2400 And 1.5 AM light are used .1.5Am are equal to one sun. By these IV characteristic it proved that it is semiconductor material with suitable band gap and it is possible to make by hydrothermal process.

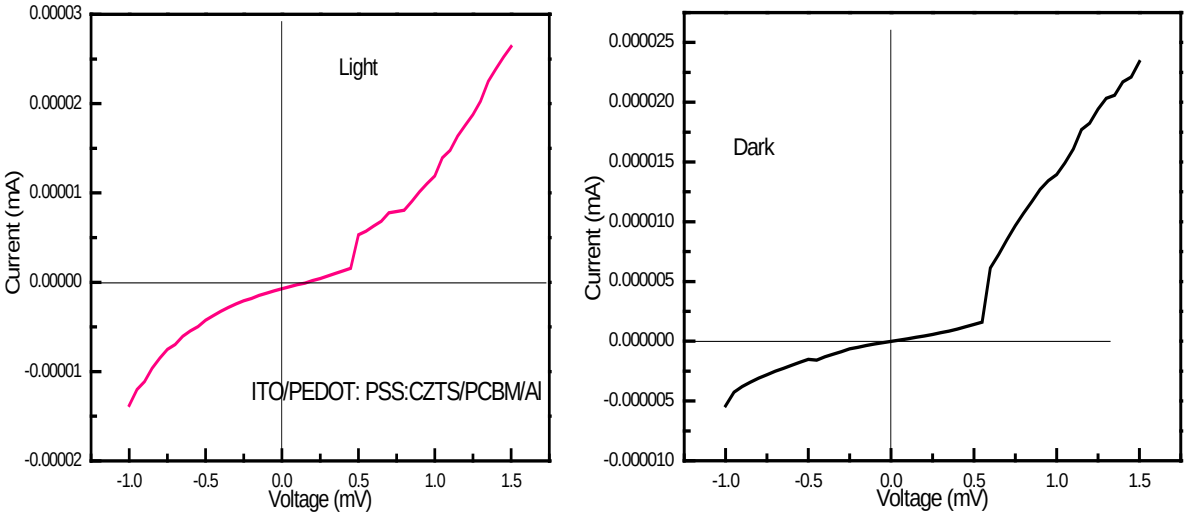


Figure 3.3.4 Shows the IV characteristics of ITO/PEDOT: PSS: CZTS/PCBM/Al both light and dark graph are shown.

# CONCLUSION CHAPTER 4

## 4.1 Conclusions

In conclusion, a solvothermal and hydrothermal synthesis of quaternary CZTS nanoparticles has been reported. Kesterite structured CZTS nano- particles with satisfactory stoichiometry and diameters in the range 5-10 and 4-8 nm obtained. The band gap of solvothermal and hydrothermal as-synthesised CZTS nanoparticles was about 1.4-1.5 eV indicating the suitable optical properties for efficient solar energy conversion. The morphologies of the continuous CZTS films with satisfactory stoichiometry were characterized by scanning electron microscopy (SEM) and energy dispersive X-ray analysis (EDXA). The crystallinity of CZTS nanoparticles was greatly improved by annealing in Nitrogen gases analyzed by X-ray diffraction (XRD). Energy-dispersive X-ray spectroscopy Energy-dispersive X-ray spectroscopy (EDX) analysis of the four constituent elements confirmed the purity and composition of CZTS nanoparticles. Composition shows that it is copper rich semiconductor material. UV–vis absorption spectra measurement indicated that the band gap of as-synthesized CZTS nanoparticles of both was about 1.5eV, which was near the optimum value for photovoltaic solar conversion in a single-band-gap device. In solar cell, IV characteristics shows photon generate when light incident.

The purpose of the presented work was to fabricate and analyse the thin film material $Cu_2ZnSnS_4$ (CZTS) and to produce solar cells based on this material. In the following the most important results are summarized.

(i) We used a two-step process to produce CZTS. The first step comprised the hydrothermal and second step solvothermal, respectively.

(ii) Analysis of the precursors showed that they were all Cu-poor and Sn-rich compared to stoichiometry (Cu/Sn in average 1.26 where 2 would be stoichiometric).

(iii) The composition was uniform within the precursors, only the surfaces showed some gradients.

(iv) For metallic precursors, crystalline phases were found, even though it was not possible to assign all XRD peaks to certain phases.

## 4.2 Future Scope

The studies presented in thesis further suggest that there are areas of academic and technological interest. These areas require further investigation. Some of the areas are mentioned as follows:

(i) A comparative study of CZTS has been done. Due to annealing process sulphur content remove so the sulphurization process used in this work was very simple and for example concerning sulphur content and pressure not controllable. Due to the simple furnace used we could sulphurize only very tiny samples which complicated the analyses in several cases.

(ii) The increase of efficiency with the Zn-content could only be shown for one fixed Cu/Sn ratio and it would be interesting to extend this study for more compositions.

(iii) Cu-rich samples will perform badly due to the secondary phase $Cu_2S$, which has to be expected according to the phase diagram.

(iv) Overall, CZTS nanoparticles were successfully synthesized via a hydrothermal route. The very low power conversion efficiencies of the hybrid solar cells investigated is an indication that the morphology problems and surfactants are still limiting factors and these problems may be overcome by using more effective using nitrogen atmosphere to solar cell. Morphological problem can be solving by using some additive to make crack less CZTS film.

# References


[1] Ingrid Repinsl, Miguel A. Contreras, Brain Egaas,Clay De Hart, John Scharf, Craig L.Perkins,BobbyToandRomenelNoufi,19.9%-efficient ZnO / CdS / CuInGaSe2 solar cell with 81.2% fill factor, Prog. Photovoltaics : Res. Appl.16 (2008)235–239.

[2] K. Ito,T. Nakazawa, Jpn. J. Appl. Phys. 27(1988) 2094.

[3] T. Tanaka, T. Nagatomo, D. Kawasaki, M. Nishio, Q. Guo, A. Wakahara, A.Yoshida, H. Ogawa, J. Phys. Chem. Solids 66 (2005) 1978.

[4] J.S. Seol, S.Y. Lee, J.C. Lee, H.D. Nam, K.H. Kim, Sol. Energy Mater. Sol. Cells 75 (2003) 155.

[5] K. Oishi, G. Saito, K. Ebina, M. Nagahashi, K. Jimbo, W.S. Maw, H. Katagiri, M.Yamazaki, H. Araki, A.Takeuchi, Thin Solid Films 517 (2008) 1449.

[6] K.Moriya, K.Tanaka, H. Uchiki, Jpn. J. Appl. Phys. 46 (2007) 5780.

[7] K.Moriya, K.Tanaka, H. Uchiki, Jpn. J. Appl. Phys. 47 (2008) 602.

[8] H. Katagiri, N. Sasaguchi, S. Hando, S. Hoshino, J. Ohashi, T. Yokota, Sol. Energy Mater. Sol. Cells 49 (1997) 407.

[9] H. Katagiri, K. Saitoh, T. Washio, H. Shinohara, T. Kurumadani, S. Miyajima, Sol. Energy Mater. Sol. Cells 65 (2001) 141.

[10] N. Kamoun, H. Bouzouita, B. Rezig,Thin Solid Films 515 (2007) 5949.

[11] Y.B. Kishore Kumar, G. Suresh Babu, P. Uday Bhaskar, V. Sundara Raja,Sol. Energy Mater. Sol. Cells 93 (2009) 1230.

[12] K. Tanaka, M. Oonuki, N. Moritake, H. Uchiki, Sol. Energy Mater. Sol. Cells 93 (2009) 583.

[13] X. Zhang, X. Shi, W. Ye, C. Ma, C. Wang, Appl. Phys. A: Mater. Sci. Process. 94 (2009) 381.

[14] X. Zhang, X.Z. Shi, W.C. Ye, C.L. Ma, C.M. Wang, Appl. Phys. A. 94 (2009) 381–386.

[15] C.Persson, J. Appl. Phys. 107 (2010) 053710-1–053710-8.

[16] G. M. Barrow, *Physikalische Chemie*, 6. Auflage, Böheimverlag, Wien (1984), 109 – 110

[17] http://www.unl.edu/CMRAcfem/temoptic.htm (13. 06. 2005)

[18] H. Hahn, H. Schulze, U¨ ber quaterna¨re chalkogenide des germaniums und zinns, Naturwissenschaften 52 (1965) 426.

[19] S.R. Hall, J.T. Szymanski, J.M. Stewart, Kesterite, Cu2(Zn,Fe)SnS4, and stannite, $Cu_2(Fe,Zn)SnS_4$, structurally similar but distinct minerals, Can. Mineral. 16 (1978) 131–137.

[20] H. Matsushita, T. Maeda, A. Katsui, T. Takizawa, Thermal analysis and synthesis from the melts of Cu-based quaternary compounds Cu-III-IV-VI4 and Cu2-II-IV-VI4 (II¼ Zn,Cd; III¼Ga,In; IV¼Ge,Sn; VI¼Se), J. Cryst. Growth 208 (2000) 416–422.

[21] G.H. Moh, Experimentelle untersuchungen an zinnkiesen und analogen germaniumverbindungen, Neues Jahrb. Mineral. Abh. 94 (1960) 1125–1146.

[22] G.H. Moh, J. Ottemann, Neue untersuchungen an zinnkiesen und zinnkiesverwandten, Neues Jahrb. Mineral. Abh. 99 (1962) 1–28.

[23] W. Sch¨ afer, R. Nitsche, Tetrahedral quaternary chalcogenides of the type Cu2-II-IV-S4(Se4), Mater. Res. Bull. 9 (1974) 645–654.

[24] S. Schorr, Structural aspects of adamantine like multinary chalcogenides, Thin Solid Films 515 (2007) 5985–5991.

[25] S.Schorr, H.-J. Hoebler, M. Tovar, A neutron diffraction study of the stannitekesterite solid solution series, Eur. J. Mineral. 19 (2007) 65–73.

[26] S.Chen, X.G. Gong, A. Walsh, S.-H.Wei, Crystal and electronic band structure of Cu2ZnSnX4 (X¼S and Se) photovoltaic absorbers: First-principles insights, Appl. Phys. Lett.94 (2009) 041903 (3 pp).

[27] I.D. Olekseyuk, L.D. Gulay, I.V. Dydchak, L.V. Piskach, O.V. Parasyuk, O.V Marchuk, Single crystal preparation and crystal structure of the Cu2Zn/Cd, Hg/SnSe4 compounds, J. Alloys Compd. 340 (2002) 141–145.

[28] R.A. Wibowo, E.S. Lee, B. Munir, K.H. Kim, Pulsed laser deposition of quaternary Cu2ZnSnSe4 thin films, Phys. Status Solidi A 204 (2007) 3373–3379.

[29] T. Maeda, S. Nakamura, T. Wada, Phase stability and electronic structure of In-free photovoltaic semiconductors,$Cu_2ZnSnSe_4$ and $Cu_2ZnSnS_4$ by first principles calculation, Mater. Res.Soc.Symp. Proc.1165 (2009) M04–03.

[30] T.K. Todorov, K.B. Reuter, D.B. Mitzi, High-efficiency solar cell with earthabundant liquid-processed absorber, Adv. Mater. 22 (2010) E156–E159.

[31] M. Himmrich, H. Haeuseler, Far infrared studies on stannite and wurtzstannite type compounds, Spectrochim. Acta 47A (1991) 933–942.

[32] H. Katagiri, N. Sasaguchi, S. Hando, S. Hoshino, J. Ohashi, T. Yokota, Preparation and evaluation of $Cu_2ZnSnS_4$ thin films by sulfurization of E-B evaporated precursors, Sol. Energy Mater. Sol. Cells 49 (1997) 407–414.

[33] K. Ito, T. Nakazawa, Electrical and optical properties of stannite-type quaternary semiconductor thin films, Jpn. J. Appl. Phys. 27 (1988) 2094–2097.

[34] J. Zhang, L. Shao, Y. Fu, E. Xie, $Cu_2ZnSnS_4$ thin films prepared by sulfurization of ion beam sputtered precursor and their electrical and optical properties, Rare Met. 25 (2006) 315–319.

[35] G. Zoppi, I. Forbes, R.W. Miles, P.J. Dale, J.J. Scragg, L.M. Peter, $Cu_2ZnSnSe_4$ thin film solar cells produced by selenisation of magnetron sputtered precursors, Prog. Photovolt.: Res. Appl. 17 (2009) 315–319.

[36] J. Krustok, R. Josepson, T. Raadik, M. Danilson, Potential fluctuations in Cu2ZnSnSe4 solar cells studied by temperature dependence of quantum efficiency curves, Physica B: Cond. Matt. 405 (2010) 3186–3189.

[37] O.V. Parasyuk, L.V. Piskach, Y.E. Romanyuk, I.D. Olekseyuk, V.I. Zaremba, V.I. Pekhnyo, Phase relations in the quasi-binary $Cu_2GeS_3$–ZnS and quasiternary $Cu_2S$–Zn (Cd)S–$GeS_2$ systems and crystal structure of $Cu_2ZnGeS_4$, J. Alloys Compd. 397 (2005) 85–94.

[38] C.-I. Lee,C.-D. Kim, Optical properties of undoped and $Co^{2+}$-doped $Cu_2Zn$ GeSe4, J. Korean Phys. Soc. 37 (2000) 364–367.

[39] S. Wagner, P.M. Bridenbaugh, Multicomponent tetrahedral compounds for solar cells, J. Cryst. Growth 39 (1977) 151–159.

[40] N.N. Konstantinova, G.A. Medvedkin, I.K. Polyshina, Y.V. Ruˇ d, A.D. Smirnova, V.I. Sokolova, M.A. Tairov, Optical and electric properties of $Cu_2CdSnSe_4$ and $Cu_2CdGeSe_4$, Inorg. Mater. 39 (1990) 1223–1226.

[41] H. Katagiri, K. Jimbo, W.S. Maw, K. Oishi, M. Yamazaki, H. Araki, A. Takeuchi, Development of CZTS-based thin film solar cells, Thin Solid Films 517 (2009) 2455–2460.

[42] Th.M.Friedlmeier, N.Wieser, Th.Walter, H. Dittrich, H.-W. Schock, Heterojunctions based on $Cu_2ZnSnS_4$ and $Cu_2ZnSnSe_4$ thin films, in: Proceedings of the 14th European Photovoltaic Solar Energy Conference, 1997,

pp. 1242–1245.

[43] B. A. Greeg, M. C. Hanna, *J. Appl. Phys.*, **93** (2003), 3605

[44] S. M. Sze: *Physics of Semiconductor Devices,* John Wiley & Sons, NewYork (1981).

[45] M. Murgia, F. Biscarini, M. Cavallini, C. Taliani, G. Ruani, *Synth. Met.*, **121** (2001), 1533

[46] D. A. Skoog - D. M. West - F. J. Holler: Fudamentals of Analytical Chemistry (Saunders College Publishing, Fort Worth, US 1992.)

[47] J. Kenkel: Analytical Chemistry for Technicians (Lewis Publishers, Boca Raton, US 1994.)

[48] Donoghue. M.(1988). A guide to manmade Gemstones, Great Britai: Van Nostrand Reinhold.

[49] T. Tanaka, D. Kawasaki, M. Nishio, Q. Guo, Hiroshi Ogawa, Phys. Status Solidi (c) 3(2006) 2844–2847.

[50] K. Tanaka, N. Moritake, H. Uchiki, Sol. Energy Mater. Sol. Cells. 91 (2007) 1199–1201.

[51] J. Seol, S. Lee, J. Lee, H. Nam, K. Kim, Sol. Energy Mater. Sol. Cells 75 (2003) 155–162

[52] J.J. Scragg, P.J. Dale, L.M. Peter, Electrochem. Commun. 10 (2008) 639–642.

[53] X. Zhang, X.Z. Shi, W.C. Ye, C.L. Ma, C.M. Wang, Appl. Phys. A. 94 (2009) 381–386.

[54] T. M. Brown, R. H. Friend, I. S. Millard, D. J. Lacey, T. Butler, J. H.Burroughes, F. Cacialli, *J. Appl. Phys.*, **93** (2003), 6159 – 6172

[55] C. J. Brabec, S. E. Shaheen, C. Winder, N. S. Sariciftci, P. Denk, *Appl.Phys. Lett.*, **80** (2002), 1288 – 1290

[56] M. Cao, Y.Shen, A mildsolvothermalroutetokesteritequaternary$Cu_2ZnSnS_4$ nanoparticles, Journal of Crystal Growth .

[57] C. Mitterbauer, *Herstellung und Charakterisierung von Bariumtitant-, Strontiumtitanat- und Magnesiumoxidschichten auf texturiertem Titan,* Diplomarbeit am Institut für Chemische Technologie Anorganischer Stoffe, Johannes Kepler Universität, Linz, (2005), 34 - 35